# CHAPTER 3

# SYNCHRONY IN RELAXATION OSCILLATORS

## 3.1 Introduction

The phrase "relaxation oscillations" was coined by van der Pol in 1926 in his analysis of a triode circuit [van der Pol, 1926]. A relaxation oscillator has two distinct time scales; a slow time scale which reflects the charging of a capacitor and a fast time scale which describes a quick discharge. The period of oscillation can be approximated by the time needed to charge the capacitor, hence the name relaxation oscillations. See Appendix A for a more detailed discussion of relaxation oscillators and their relation to sinusoidal type oscillators.

Relaxation oscillators were immediately recognized as having similarities to biological oscillators. Van der Pol and van der Mark may have been the first to use relaxation oscillators to model biological phenomena [van der Pol and van der Mark, 1928]. In 1952 Hodgkin and Huxley gave a mathematical model of the membrane potential and ionic conductances of a nerve cell using a four variable system of differential equations [Hodgkin and Huxley, 1952]. This famous system of equations was later simplified to a two variable system of equations that is essentially a relaxation oscillator [Fitzhugh, 1961, Nagumo et al., 1962]. Later, Mayeri [Mayeri, 1973] derived the van der Pol relaxation oscillator as a quantitative description of his experiments with the cardiac ganglion cells of the lobster. Morris and Lecar [Morris and Lecar, 1981] also derived a two variable relaxation type oscillator in their study of the conductances and currents in the barnacle giant muscle fiber. Due to these direct links to neurophysiology, relaxation oscillators have been frequently examined as models of neural behavior [Grasman and Jansen, 1979, Plant, 1981, Grossberg and Somers, 1991, Somers and Kopell, 1993, Terman and Wang, 1995].

Synchrony in networks of relaxation oscillators has been studied previously. Somers and Kopell [Somers and Kopell, 1993] and independently Wang [Wang, 1993a] both noted that synchrony occurs more rapidly in locally coupled networks of identical relaxation oscillators than in networks of locally coupled sinusoidal oscillators. Terman and Wang [Terman and Wang, 1995] proved that a network of locally coupled identical relaxation oscillators with a Heaviside type interaction can achieve synchrony at an exponential

rate independent of the number of oscillators or the dimension of the network. However, this rate of synchronization is possible only when the oscillators are initially on a specific portion of the limit cycle.

We examine the rate of synchrony in such networks in which the oscillators can be placed anywhere on the limit cycle. This results in a fundamental change in average time needed to achieve synchrony. For one-dimensional noiseless networks in the singular limit ($\varepsilon = 0$, also see Section 3.3.1 and Appendix A), we find that the average time to synchrony, $\langle T_S \rangle$, is proportional to $n^p$, where $n$ is the size of the system and $p$ is a numerically obtained value that is less than 0.5 and is dependent on system parameters. For two-dimensional networks of relaxation oscillators, our results are not conclusive, but for appropriate parameter choices we observe that $\langle T_S \rangle$ increases logarithmically with the system size.

One-dimensional networks of locally coupled identical relaxation oscillators exhibit other behaviors besides synchrony. There are two types of desynchronous solutions, fractured synchrony and travelling waves. We derive explicit conditions needed for the formation of fractured synchrony and we provide a detailed explanation of the conditions necessary for the formation of travelling waves. In two dimensional networks, additional spatiotemporal patterns arise, including rotating waves. We give examples of some spatiotemporal patterns and describe initial conditions and parameters which can inhibit or enhance their formation.

Relaxation oscillators also share some similarities with the integrate-and-fire oscillators discussed in Chapter 2. Both types of oscillators have two distinct time scales and both are typically studied with a nonlinear, asymmetric interaction. Because of these similarities, integrate-and-fire oscillators and relaxation oscillators are thought to share many properties. But, there are differences. For example, relaxation oscillators have interactions of finite duration. Our analysis of relaxation oscillators indicates how to modify parameters so that relaxation oscillators have properties associated with integrate-and-fire type oscillators.

For one-dimensional networks of identical relaxation oscillators with $\varepsilon > 0$ and a Heaviside type interaction, Somers and Kopell [Somers and Kopell, 1993] suggested that the average time to synchrony increases linearly with $n$. However, it is not known whether this scaling relation is due to the fact that the oscillators are relaxation type, or because the interaction is discontinuous. We present numerical evidence suggesting that the interaction can result in this scaling relation, independent of the type of oscillator used. This provides further evidence [see Chapter 2, Daido, 1993b] that a discontinuous interactions can qualitatively change the properties of synchronization in oscillator networks when compared with smooth, continuous interactions.

This Chapter is organized as follows. In Section 3.2 we briefly describe a single relaxation oscillator. We then describe a pair of interacting relaxation oscillators and detail how we perform analysis in the singular limit ($\varepsilon = 0$) in Section 3.3. We discuss desynchrony in one-dimensional chains of oscillators in Section 3.4, which contains a detailed examination of fractured synchrony and travelling waves. In Section 3.5 we discuss our data on synchrony in one-dimensional networks of relaxation oscillators. We attempt to explain the observed scaling relationship and we also examine the sensitivity of these systems to spin wave type initial conditions. Section 3.6 displays our data on both synchrony and

spatiotemporal pattern formation in two-dimensional networks. In Section 3.7 we compare the average time to synchrony in one-dimensional networks of integrate-and-fire oscillators with that of networks of relaxation oscillators. In Section 3.8 we present data for the average time to synchrony in one-dimensional networks of relaxation oscillators that are not in the singular limit ($\varepsilon > 0$) using both smooth and discontinuous interactions. Section 3.9 concludes the Chapter.

## 3.2 A Single Relaxation Oscillator

The relaxation oscillators we use are equivalent to the Terman-Wang relaxation oscillator [Terman and Wang, 1995]. This oscillator is closely related to the model of neuronal oscillation derived by Morris and Lecar [Morris and Lecar, 1981], but is considerably simpler. Locally coupled networks of these oscillators have been shown to achieve synchrony more rapidly than networks consisting of other types of oscillators [Somers and Kopell, 1993]. A single relaxation oscillator is defined as

$$\dot{x} = 3x - x^3 - y \tag{3.1.a}$$

$$\dot{y} = \varepsilon ( \lambda + \gamma \tanh(\beta x) - y ) \tag{3.1.b}$$

The limit cycle and nullclines for this oscillator are shown in Figure 17. The x-nullcline, $\dot{x} = 0$, is a cubic function. Two important values of this cubic are the y-values of the local extrema, denoted by ***RK*** (right knee) and ***LK*** (left knee). The y-nullcline, $\dot{y} = 0$, is a sigmoid and is assumed to be below the left branch (LB) and above the right branch (RB) of the cubic as shown in Figure 17. The parameter $\beta$ controls the steepness of the sigmoid and we use $\beta \gg 1$. The value $\varepsilon$ is chosen to be small, $0 < \varepsilon \ll 1$, so that motion in the x-direction is fast in comparison to motion in the y-direction. The oscillator thus defined is a typical relaxation oscillator. The limit cycle is made up of four pieces: two slowly changing pieces along the left and right branches of the cubic and two fast pieces that connect the left and right solutions. The parameters $\lambda$ and $\gamma$ are used to modify the amount of time an oscillator spends on the left and right branches. We assume that the amount of time an oscillator needs to traverse the left branch is larger than the amount of time it needs to traverse the right branch. The left and right branches are referred to as the silent and active phases of the limit cycle.

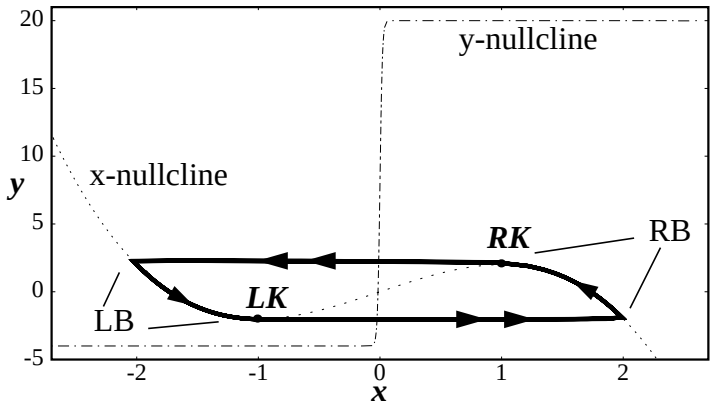


Figure 17. A plot of the nullclines and limit cycle of a relaxation oscillator. The dotted curve is the x-nullcline and the dash-dot curve is the y-nullcline. The limit cycle is given by the thick dark curve. The abbreviations are described in the text. The parameters used are $\lambda = 8$, $\gamma = 12$, $\varepsilon = 0.005$, and $\beta = 1000$.

## 3.3 A Pair of Relaxation Oscillators

We now examine two coupled relaxation oscillators, defined as

$$\dot{x}_1 = 3x_1 - x_1^3 - y_1 + \alpha_R S(x_2) \tag{3.2.a}$$

$$\dot{y}_1 = \varepsilon ( \lambda + \gamma \tanh(\beta x_1) - y_1 ) \tag{3.2.b}$$

$$\dot{x}_2 = 3x_2 - x_2^3 - y_2 + \alpha_R S(x_1) \tag{3.2.c}$$

$$\dot{y}_2 = \varepsilon ( \lambda + \gamma \tanh(\beta x_2) - y_2 ) \tag{3.2.d}$$

$$S(x) = [\, 1 + \exp(\kappa (\theta - x)) \,]^{-1} \tag{3.2.e}$$

The parameter $\alpha_R$ is the coupling strength and is assumed to be positive. The subscript $R$ denotes that this is the coupling strength between relaxation oscillators. The interaction term is a sigmoid, mimicking excitatory chemical synapses. Increasing the value of $\alpha_R S(x)$ elevates the x-nullcline, $\dot{x}_i = 0$. This is a property seen in several descriptions of neural behavior [Hodgkin and Huxley, 1952, Fitzhugh, 1961, Wilson and Cowan, 1972, Morris and Lecar, 1981]. Because the parameter $\kappa \gg 1$, the interaction is approximately a binary function. The threshold of the interaction term, $\theta$, is placed between the left and right branches of the x-nullcline, thus the interaction term is either on or off depending on whether or not an oscillator is on the active or silent phase of the limit cycle. When one oscillator, $O_1$, is on the right branch, the other oscillator, $O_2$, is said to receive excitation. This excitation raises the x-nullcline of $O_2$, now called the excited, or upper nullcline, and

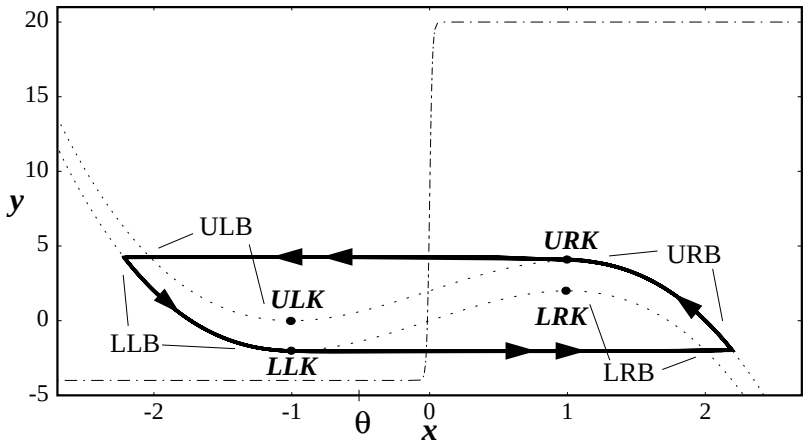


Figure 18. A plot of the nullclines and limit cycle for a pair of synchronous relaxation oscillators. The two dotted curves represent the two x-nullclines of this system and the dash-dot curve is the y-nullcline. The limit cycle is given by the thick dark curve. The parameters used are $\alpha_R = 2$ and the other parameters are as listed in Figure 17. The

$O_2$ now exhibits dynamics based on its modified phase space. The three nullclines for this system and the limit cycle of the synchronous solution are shown in Figure 18. The pertinent values of the x-nullclines are the y-values of their local extrema. For the particular equations we use in (3.2), the x-nullcline shifts upward in direct proportion to $\alpha_R S(x)$. The four local extrema are denoted by the lower left knee (***LLK***) and the lower right knee (***LRK***) for the unexcited x-nullcline, and the upper left knee (***ULK***) and the upper right knee (***URK***) for the excited nullcline. The values of the extrema for the x-nullclines given in (3.2) are

$$\boldsymbol{LLK} = (LLK_x, LLK_y) = (-1, -2)$$

$$\boldsymbol{LRK} = (LRK_x, LRK_y) = (1, 2)$$

$$\boldsymbol{ULK} = (LLK_x, LLK_y + \alpha_R)$$

$$\boldsymbol{URK} = (LRK_x, LRK_y + \alpha_R)$$

The synchronous solution for a pair of oscillators is shown in Figure 18. Because of the interaction, the oscillators travel a larger distance along the cubics than when uncoupled and therefore the synchronous solution has a longer period than a single uncoupled oscillator. When an oscillator is on either of the left branches, we say that it is in the silent phase and when an oscillator is on either of the right branches, we say that it is in the active phase.

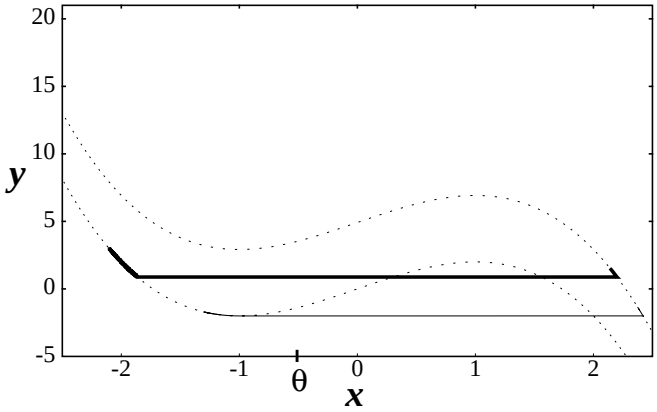


Figure 19. An example of the trajectories for a pair of coupled relaxation oscillators. The thin solid curve represents the first oscillator to jump and the thick solid curve represents the oscillator that receives excitation. The two dotted curves are the excited and unexcited cubics. The parameters are the same as in Figure 18 with $\alpha_R = 6.0$.

In Figure 19 we display an example of the trajectories for two coupled oscillators, as well as the excited and unexcited x-nullclines; both oscillators are initially placed on the lower left branch. The trajectory of $O_1$ is shown by the thin curve and that of $O_2$ is shown by the thick curve. $O_1$ travels until it reaches the lower left knee. When it reaches this knee, it begins to move in the positive x-direction. Motion in the x-direction occurs quickly in relation to motion in the y-direction (or instantly if $\varepsilon = 0$). This motion is referred to as a "jump up" from the silent to the active phase. As $O_1$ jumps up, its x-value crosses the threshold of the interaction, $\theta$, and $O_2$ receives excitation. The interaction term elevates the x-nullcline of $O_2$ by $\alpha_R$. When its x-nullcline rises, $O_2$ is suddenly below the upper left knee and is induced to jump up. The range of initial conditions for which this can occur is called the jumping region, and this jumping region is analogous to the jumping region described for integrate-and-fire oscillators (see Section 2.2). Note that when the two oscillators jump up together, the y-distance between them does not change. Because of this, we use the reset rule for integrate-and-fire oscillators given in (2.4), which does not alter the Euclidean distance between two integrate-and-fire oscillators when they fire synchronously. It has been shown that a locally coupled network of relaxation oscillators, with initial conditions such that all oscillators can jump up together, synchronizes at a geometric rate [Terman and Wang, 1995].

Figure 19 diagrams just one class of trajectories that a pair of coupled relaxation oscillators can exhibit. There are other trajectories for the two relaxation oscillators dependent on their initial conditions. For example, $O_2$ can have an initial condition such that it is not able to jump immediately when it receives excitation and instead "hops" from the lower left branch to the upper left branch. Somers and Kopell [Somers and Kopell, 1993] originally described several classes of these trajectories (shown in Appendix A2). For the particular relaxation oscillator we study, these classes of trajectories have been analyzed by Campbell and Wang [Campbell and Wang, in press]. Although we examined time delays,

the results they obtained are valid for zero time delay and are derived in Appendix B. If there is no time delay in the interaction, then synchrony is the asymptotically approached solution for all initial conditions in which both oscillators start on the lower left branch of the limit cycle and if coupling strength satisfies (B.35). In Section 3.3.1 we describe how to analytically examine the trajectories of a pair of relaxation oscillators in the singular limit.

If the coupling strength is not large enough, then a pair of relaxation oscillators can have stable desynchronous solutions [Kopell and Somers, 1995]. We explicitly derive the minimum coupling strength needed for synchrony in a pair of coupled Terman-Wang oscillators in Appendix B. When dealing with one-dimensional networks of relaxation oscillators, another constraint on the coupling strength arises. We explain this constraint and explicitly derive the minimum coupling strength needed to prohibit these desynchronous solutions in Section 3.4.1. For all synchronization results in this paper, we use a coupling strength that always results in synchrony. Note that a pair of pulse-coupled integrate-and-fire oscillators become synchronous with any positive coupling strength [Mirollo and Strogatz, 1990].

### 3.3.1 Relaxation Oscillators in the Singular Limit

We now describe how the trajectories for coupled relaxation oscillators can be analytically computed. In the singular limit, when $\varepsilon = 0$, the motion of an oscillator can be determined by a single variable and the knowledge of which branch the oscillator is on (see [Terman and Wang, 1995]). We derive these statements below.

We examine the two oscillators defined in (3.2),

$$\dot{x}_1 = 3x_1 - x_1^3 - y_1 + \alpha_R S(x_2) \tag{3.3.a}$$

$$\dot{y}_1 = \varepsilon(\lambda + \gamma \tanh(\beta x_1) - y_1) \tag{3.3.b}$$

$$\dot{x}_2 = 3x_2 - x_2^3 - y_2 + \alpha_R S(x_1) \tag{3.3.c}$$

$$\dot{y}_2 = \varepsilon(\lambda + \gamma \tanh(\beta x_2) - y_2) \tag{3.3.d}$$

$$S(x) = [\,1 + \exp(\kappa(\theta - x))\,]^{-1} \tag{3.3.e}$$

The fast system of (3.3) is obtained by setting $\varepsilon = 0$. This results in

$$\dot{x}_i = 3x_i - x_i^3 - y_i + \alpha_R S(x_j(t)) \tag{3.4.a}$$

$$\dot{y}_i = 0 \tag{3.4.b}$$

where $i = 1, 2$ and $j = 3 - i$. The slow system for (3.3) is derived by introducing a slow time scale $t' = \varepsilon t$ and then setting $\varepsilon = 0$. The slow system for the lower left branch is

$$x_i = h(y_i) \tag{3.5.a}$$

$$\dot{y}_i = \lambda + \gamma \tanh[\beta h(y_i)] - y_i \tag{3.5.b}$$

where $x = h(y)$ describes the lower left branch of (3.3). System (3.5) determines the slow evolution of an oscillator on the lower left branch. Because $\beta \gg 1$ and $h(y) \leq -1$, we rewrite (3.5.b) as

$$\dot{y}_i = \lambda - \gamma - y_i \tag{3.6}$$

For an oscillator on the upper left branch, (3.6) will again result because $h_e(y) \leq -1$, where $x = h_e(y)$ defines the upper left branch. Thus, because the y-nullcline is step-like, an oscillator has the same velocity in the y-direction along either of the left branches. For the right branches, these same steps result in the following analogous equation,

$$\dot{y}_i = \lambda + \gamma - y_i \tag{3.7}$$

The velocity in the y-direction of an oscillator along either of the right branches is given by (3.7). This type of analysis can be done for other relaxation oscillators as well. In more generalized versions of relaxation oscillators, the speed along different cubics may be different.

In the singular limit, $\varepsilon = 0$, system (3.3) reduces to two variables. The exact form of the x-nullcline is not important as long as a general cubic shape is maintained. The evolution of the system is determined through the knowledge of the location of the local extrema and by solving (3.6) and (3.7). The equation describing $y_i(t)$ along either of the left branches is

$$y_i(t) = (y_i(0) - \lambda + \gamma)\, e^{-t} + \lambda - \gamma \tag{3.8}$$

The y-position of an oscillator along either of the right branches is given by

$$y_i(t) = (y_i(0) - \lambda - \gamma)\, e^{-t} + \lambda + \gamma \tag{3.9}$$

We compute the total period of oscillation, $P_T$, for the synchronous solution using (3.8) and (3.9). The time it takes to travel from $LLK_y$ to $LRK_y + \alpha_R$, along the upper right branch, is given by

$$\tau_{URB} = \log\left( \frac{LLK_y - \gamma - \lambda}{LRK_y + \alpha_R - \gamma - \lambda} \right) \tag{3.10}$$

The time needed to travel from $LRK_y + \alpha_R$ to $LLK_y$, along the lower left branch, is given by

$$\tau_{LLB} = \log\left(\frac{LRK_y + \alpha_R + \gamma - \lambda}{LLK_y + \gamma - \lambda}\right) \tag{3.11}$$

Thus, we have $P_T = \tau_{URB} + \tau_{LLB}$. The period of the synchronous solution for two coupled oscillators is greater than the period of a single uncoupled oscillator, because the coupling always has an effect even if the oscillators are perfectly synchronous. Thus the synchronous period is a function of the coupling strength. As mentioned previously, the amount of time an oscillator spends in the silent phase is larger it does in the active phase. This will become an important consideration in later sections. We define the branch ratio, $B_r$, as the time an oscillator spends on the lower left branch divided by the time it spends on the upper right branch,

$$B_r = \frac{\tau_{LLB}}{\tau_{URB}} \tag{3.12}$$

The branch ratio also gives a qualitative measure of how the speeds along the left and right branches differ since both branches have the same length in the y-direction.

Our analyses in this Chapter and in Appendix B are derived at the singular limit, i.e. $\varepsilon = 0$. We have not carried out a perturbation analysis, but we note that Terman and Wang [Terman and Wang, 1995] have carried out an analysis of networks of relaxation oscillators in the singular limit and extended their analysis from $\varepsilon = 0$ to small positive $\varepsilon$. Our networks do not differ from theirs, so our results should also be valid for small positive $\varepsilon$. We have confirmed this with substantial simulations using various values of $\varepsilon$. Our results indicate that values of $0 < \varepsilon \ll 1$ do not significantly alter any of the trajectories discussed for a pair of oscillators. However, a finite value of $\varepsilon$ does change the scaling relation between the time to synchrony and the size of the system. We discuss this issue in Section 3.8.

In studying relaxation oscillators, it is useful to have some measure of the distance between them. We characterize the separation between the two oscillators by using the time difference between them, $\Gamma(y_1, y_2)$, which is defined as

$$\Gamma(y_1, y_2) = \begin{cases} \log\left(\dfrac{y_2 - \lambda + \gamma}{y_1 - \lambda + \gamma}\right) & \textit{if both oscillators on left branch} \\ \log\left(\dfrac{y_2 - \lambda - \gamma}{y_1 - \lambda - \gamma}\right) & \textit{if both oscillators on right branch} \end{cases} \tag{3.13}$$

where $y_i$ is the y-value of $O_i$. This function represents the time needed for $y_2$ to travel to the position of $y_1$. This function is valid only if both oscillators are on the silent (or active) phase of the limit cycle and is undefined otherwise. We use the time difference between the two oscillators as a description of their relationship because this quantity is invariant when the two oscillators are on the same branch of the system [LoFaro, 1994, Terman and Wang, 1995].

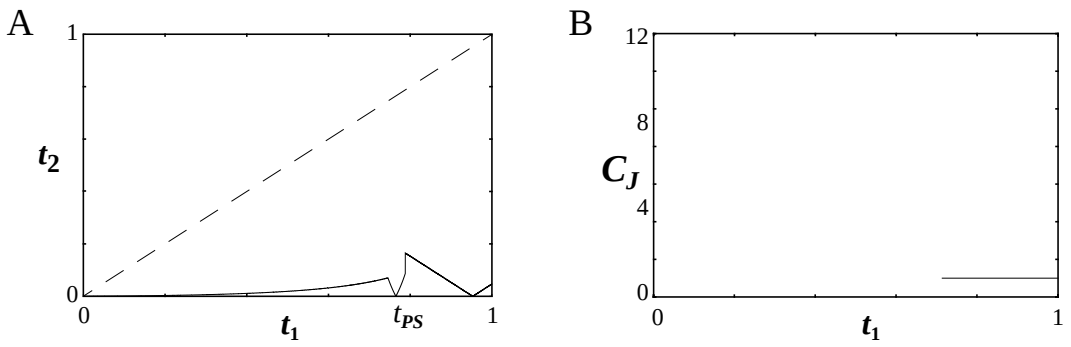


Figure 20. (A) The return map for two relaxation oscillators. The horizontal axis represents the initial time difference, $t_1$, between the two oscillators on the lower left branch and the vertical axis represents the time difference between the two oscillators when they are next on the lower left branch, $t_2$. (B) A plot of the number of periods needed before both oscillators are in the jumping region, $C_J$, as a function of the initial time difference between the two oscillators, $t_1$. The parameters used are given in the Figure 18 caption.

We use the equations derived in Appendix B to calculate a return map (Figure 20A) for a pair of oscillators initially placed on the lower left branch. The initial time difference between the two oscillators is represented on the horizontal axis. The vertical axis displays the time difference between the two oscillators the next time they are both on the lower left branch. This return map ignores changes in ordering which occur. We note several features of this return map. The jumping region is given by the first 70% of the initial conditions. Just beyond the jumping region, there is an initial time difference, $t_{PS}$, which results in perfect synchrony between the two oscillators. Somers and Kopell [Somers and Kopell, 1993] called the region near this time difference "supercompressed", because large initial time differences are mapped, or compressed, into very small time differences in just one period. For larger initial time differences, the first oscillator can jump up, and traverse the lower right branch before the other oscillator can jump up. For the parameters we use, this trajectory also results in a significant reduction in the time difference. In Figure 20B we display the number of periods that are needed before the two oscillators are in the jumping region as a function of their initial time difference. The maximum number of cycles needed before both oscillators jump up together is one.

Although we have performed analysis only for initial conditions such that both oscillators start on the lower left branch, all of our computer simulations indicate that synchrony is achieved in a pair of oscillators even if both oscillators are randomly distributed on both branches of the limit cycle (if the coupling strength is large enough). This observation has also been made by Somers and Kopell [Somers and Kopell, 1993, Terman and Wang, 1995].

We now describe another aspect of a pair of relaxation oscillators. For two oscillators we define the compression ratio, $C_R$. This term is a multiplicative factor that is less than one and describes how the time difference between the two oscillators changes when they jump up and down together. The largest value of $C_R$ for system (3.3) is given by the following quantity,

$$C_R = \frac{\log\left(\frac{c_4}{c_8}\right)\log\left(\frac{c_5}{c_1}\right)}{\log\left(\frac{c_2}{c_6}\right)\log\left(\frac{c_7}{c_3}\right)} \tag{3.14}$$

where the values of $c_i$ are given by

$$\begin{aligned} c_1 &= LLK_y - \lambda - \gamma & c_5 &= LLK_y + \alpha_R - \lambda - \gamma \\ c_2 &= LLK_y - \lambda + \gamma & c_6 &= LLK_y + \alpha_R - \lambda + \gamma \\ c_3 &= LRK_y - \lambda - \gamma & c_7 &= LRK_y + \alpha_R - \lambda - \gamma \\ c_4 &= LRK_y - \lambda + \gamma & c_8 &= LRK_y + \alpha_R - \lambda + \gamma \end{aligned} \tag{3.15}$$

It can be shown that (3.14) has its minimum value when $B_r = 1$, i.e. when the amount of time an oscillator spends in the active phase is equal to the amount of time it spends in the silent phase. When $B_r = 1$ a pair of oscillators has the smallest value of $C_R$. Both $B_r$ and $C_R$ will play a role in the rate of synchronization in one-dimensional chains of relaxation oscillators.

In summary, we described the dynamics of a pair of relaxation oscillators with a Heaviside type coupling. We have shown how analysis is performed in the singular limit and we have shown that synchrony is the asymptotically approached solution for a broad range of initial conditions. We have also described that desynchronous solutions exist if the coupling strength is not large enough.

## 3.4 Desynchrony in One-Dimensional Networks

In a pair of relaxation oscillators, there are two types of behaviors, a synchronous solution that arises if the coupling strength is large enough, and a desynchronous solution that can occur otherwise. One-dimensional networks of oscillators exhibit two analogous behaviors and a third dynamic which is a travelling wave. A network of relaxation oscillators is called synchronous if all the oscillators jump up (or down) at the same time. It is described as exhibiting fractured synchrony (following the terminology of Kopell and Somers [Kopell and Somers, 1995]) if groups of oscillators exist that have desynchronous relations with each other because the coupling strength is not large enough. We examine fractured synchrony in Section 3.4.1. The third behavior, travelling waves, only occur in networks of oscillators with a ring topology and we examine this behavior in Section 3.4.2.

### 3.4.1 Fractured Synchrony in Chains of Relaxation Oscillators

We first define a network of *n* relaxation oscillators as follows,

$$\dot{x}_i = 3x_i - x_i^3 - y_i + \sum_{j \in N(i)} J_{ij} S(x_j) \tag{3.16.a}$$

$$\dot{y}_i = \varepsilon (\lambda + \gamma \tanh(\beta x_i) - y_i) \tag{3.16.b}$$

$$S(x) = [1 + \exp(\kappa (\theta - x))]^{-1} \tag{3.16.c}$$

The sum is over all the nearest neighbors, $N(i)$, of oscillator $i$. As in networks of integrate-and-fire oscillators, the coupling strengths are normalized using

$$J_{ij} = \frac{\alpha_R}{Z_i} \tag{3.17}$$

where $Z_i$ is the number of nearest neighbors that oscillator $i$ has. This normalization ensures that all the oscillators have the same trajectory in phase space when synchronous regardless of how many neighbors they have [Wang, 1995].

As mentioned previously, a pair of oscillators do not achieve synchrony for all initial conditions on the lower left branch if the coupling strength is not large enough [Kopell and Somers, 1995]. For system (3.3) we derive this condition in Appendix B. When dealing with a one-dimensional chain of oscillators a similar constraint arises; desynchronous solutions can arise if the coupling strength is not large enough.

In a one-dimensional chain of oscillators there are three pertinent x-nullclines that an oscillator may lie on, dependent on whether it receives excitation from zero, one, or two of its neighboring oscillators. In Figure 21A we display a portion of the trajectories of two neighboring oscillators which have a desynchronous relation in a chain of oscillators. One oscillator, $O_1$, receives excitation and jumps up to the right middle branch. It quickly travels the length of this branch and jumps down to the middle left branch. When $O_1$ sends excitation to $O_2$, $O_2$ hops to the middle left branch. $O_2$ receives excitation only for a time

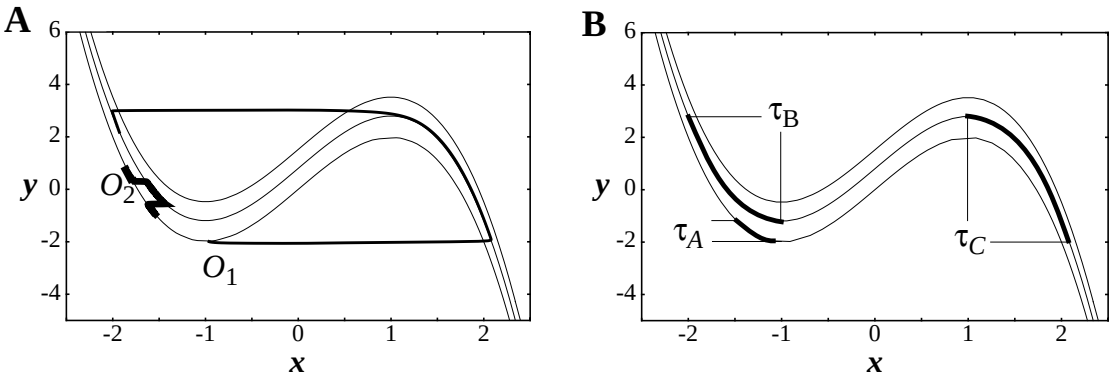


Figure 21. (A) The trajectories of two neighboring oscillators that have a desynchronous relation in a chain of oscillators. (B) The three pertinent portions of the x-nullclines which play a role in the desynchronous solutions. The symbols $\tau_A$, $\tau_B$, and $\tau_C$ represent the time needed to traverse the indicated portions of the cubics.

$\tau_C$ and it hops back down to the lower left branch when it ceases to receive excitation. This process repeats if $O_2$ is able to travel down to the lower left knee, a minimum time of $\tau_A$, and traverse the right middle branch, a time of $\tau_C$, before $O_1$ can traverse the length of the left middle branch, which takes a time $\tau_B$. The portions of the nullclines that correspond to these constants ($\tau_A$,$\tau_B$,$\tau_C$) are shown in Figure 21B. In order to prevent desynchronous solutions, the following condition must hold

$$\tau_A + \tau_C > \tau_B \tag{3.18}$$

For system (3.16) (with $\varepsilon = 0$) these time constants can be found explicitly as shown in the Section 3.3.1. Condition (3.18) becomes

$$\frac{c_2 c_7}{c_6 c_1} < \frac{c_6}{c_8} \tag{3.19}$$

where the values of $c_i$ are given in (3.15). Condition (3.19) can be rewritten as a function of $\alpha_R$,

$$\alpha_R^2 (c_2 - c_1) + \alpha_R (c_2 c_3 + c_2 c_4 - 2 c_1 c_2) + c_2 c_3 c_4 - c_1 c_2^2 < 0 \tag{3.20}$$

This results in the following relationship between $\alpha_R$ and the other system parameters,

$$\alpha_R > \frac{-(c_2 c_3 + c_2 c_4 - 2 c_1 c_2)}{2 (c_2 - c_1)} + \frac{\sqrt{(c_2 c_3 + c_2 c_4 - 2 c_1 c_2)^2 - 4 (c_2 - c_1) (c_2 c_3 c_4 - c_1 c_2^2)}}{2 (c_2 - c_1)} \tag{3.21}$$

If condition (3.21) is satisfied then these desynchronous solutions do not occur in one-dimensional networks. Numerical tests verify the above condition on the coupling strength. Let us denote the minimum coupling strength needed to satisfy (3.21) as the critical coupling strength, $\alpha_R^C$. If $\alpha_R$ is less than $\alpha_R^C$, then some range of initial conditions exist in which neighboring oscillators can have a desynchronous relationship. For each initial condition within this range, there is a corresponding trajectory for a desynchronous solution. Thus these solutions are neutrally stable. This neutral stability results from the fact that the speed of motion in the y-direction is the same along all of the left branches. If the speed of motion in the y-direction is different for the different branches (a more general case) then an analysis similar to that by Kopell and Somers [Kopell and Somers, 1995] can indicate how the stability of desynchronous solutions is related to the different speeds of motion along the different branches. Because these desynchronous oscillators do not travel along the same path as the synchronous solutions, their frequency is different. The frequency of these desynchronous solutions is

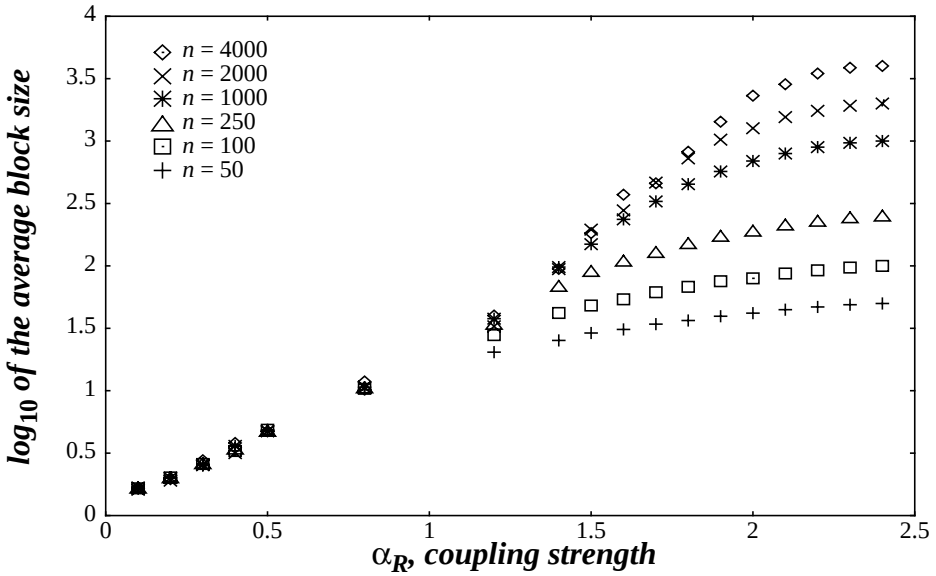


Figure 22. The average block size as a function of the coupling strength for several chains of length $n$. The parameters used are $\lambda = 9$ and $\gamma = 12$. The critical coupling strength is $\alpha_R^C = 2.3786$ using (3.18). Each point represents the average block size calculated from several hundred trials with random initial conditions.

$$P_D = \log\left(\frac{c_1}{c_3 + \alpha_R/2}\right) + \log\left(\frac{c_4 + \alpha_R/2}{c_2}\right) \tag{3.22}$$

and this has been confirmed by simulations.

If the coupling strength does not satisfy condition (3.21) then two oscillators in a chain can have a desynchronous relation. This requires that the two oscillators have a specific spatiotemporal relationship on the limit cycle and further, that this relationship is maintained as the two desynchronous neighboring oscillators interact with their other neighbors. Thus, even if the coupling is less than the critical coupling strength, it is possible that a chain of oscillators with random initial conditions can exhibit synchrony. It is also possible that, occasionally, two oscillators will be desynchronous and create a boundary between two clusters, or blocks, of synchronous oscillators. Kopell and Somers refer to this formation of blocks of synchronous oscillators as fractured synchrony [Kopell and Somers, 1995].

Fractured synchrony arises only when the coupling strength is small enough and when two neighboring oscillators in the network have the correct relative positions on the x-nullclines to remain in a desynchronous relationship. As $\alpha_R$ increases, the range of initial conditions which result in desynchronous solutions decreases and one expects that the average block size must increase. How the average block size increases in relation to the coupling strength is an intriguing question. In Figure 22 we display our numerical data on how the average block size increases as a function of $\alpha_R$ for networks of different sizes. The data indicate that the average block size (for blocks of size less than 10) forms inde-

pendent of the system size. For larger values of the coupling strength, the average block size becomes dependent on the size of the system, which is expected because the block size is limited by the size of the system. For an infinite system, the function describing the relationship between the average block size and $\alpha_R$ must diverge at the critical coupling strength, $\alpha_R^C$. One can fit the lower portion of the curves in Figure 22 well with a function of the form

$$\frac{e^{3\alpha_R}}{(\alpha_R^C - \alpha_R)^{-3}} \tag{3.23}$$

This function diverges at the critical coupling strength but we have no theoretical understanding of how (3.23) arises. Also, we have not been able to accurately estimate the functional form for finite size systems.

All data were obtained for relaxation oscillators in the singular limit ($\varepsilon = 0$). The trajectories of the oscillators were computed numerically using the algorithm developed by Linsay and Wang called the singular limit method [Linsay and Wang, 1996], which is much faster than traditional methods of numerical integration.

### 3.4.2 Travelling Waves in Rings of Relaxation Oscillators

In the previous section we derived a condition that prohibits fractured synchrony in one-dimensional networks of relaxation oscillators. This is not a sufficient condition for synchrony and we find that other behaviors arise besides synchrony. Travelling waves may develop if the network is a ring instead of a chain of oscillators (also observed by [Somers and Kopell, 1993]). We graphically describe these travelling waves for one-dimensional systems below and this analysis allows us to derive their frequency as well as approximate the minimum number of oscillators necessary to form a travelling wave.

In Figure 23 we display a few snapshots in time of a travelling wave. The x- and y-positions of 16 oscillators are shown, as well as the three nullclines that each oscillator can lie on. The initial conditions are specifically chosen so that a travelling wave results. Oscillator B is coupled to oscillators A and C. Oscillator C is coupled with oscillators B and D and each oscillator on the left branches is coupled to its nearest neighbors. Some of the oscillators have synchronized and their dots overlap. The speed of motion along the left and right branches are quite different, i.e. $B_r = 5.14$. Thus, even though the Euclidean distance between two oscillators on the active phase is greater than that between two oscillators on the silent phase, their time differences are very similar. Figure 23A shows the locations of the oscillators just before oscillator B jumps up and Figure 23B shows the system just after oscillator B jumps up. Oscillator B sends excitation to both oscillators C and A. As a result oscillator C hops from the middle right branch to the upper right branch and oscillator A hops from the lower left branch to the middle left branch. Figure 23C shows the positions of the oscillators when oscillator D has just jumped down to the lower middle branch. As a result, oscillator E hops down from the middle left branch to the lower left branch and oscillator C hops down from the upper right branch to the middle right branch. For a few moments in time there are only two oscillators on the right

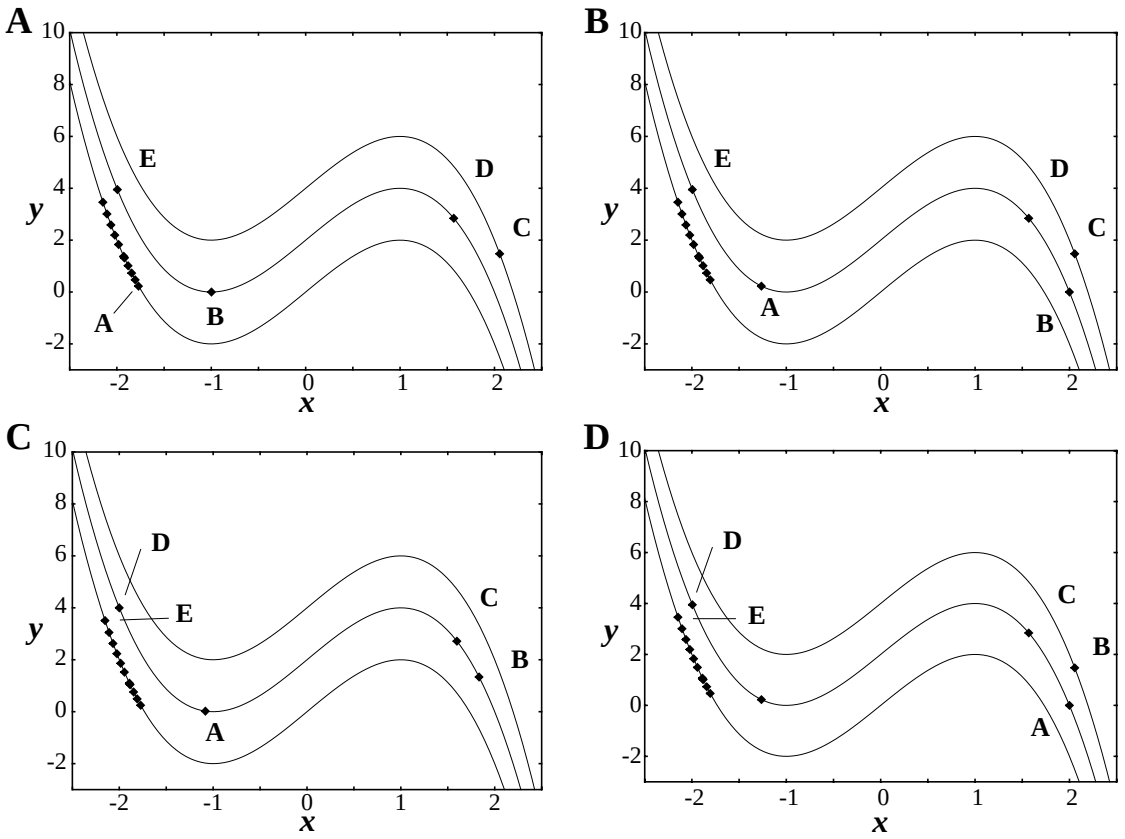


Figure 23. The positions of 16 oscillators in a travelling wave are shown at four different instants in time. The time slices are shown in consecutive order in (A), (B), (C), and (D). The network is a one-dimensional ring. The parameters are $\lambda = 9$, $\gamma = 12$, and $\alpha_R = 4$.

branches and then oscillator A jumps up. This configuration is shown in Figure 23D, which is nearly identical to Figure 23B. Because the oscillators have appropriate spatial locations, the sequence of events shown in Figure 23 is able to repeat.

An important point about travelling waves is that the time difference between oscillators does not change. Figure 23A represents the oscillators just before oscillator B jumps up; there is some y-distance between oscillator A and the middle left knee (the position of oscillator B). When oscillator B jumps up, oscillator A is induced to hop to the middle left branch and must traverse this same y-distance before it can jump up. Because the oscillators traverse the same y-distance, their time difference does not change. The time differences between all oscillators in this travelling wave are maintained and thus the travelling wave cycles endlessly.

The period of this travelling wave is different from the synchronous period because the oscillators never traverse the entire length of the outer branches. They only traverse the length of the middle left and right branches and this period is given by

$$P_M = \tau_B + \tau_C = \log\left(\frac{c_4 + \alpha_R/2}{c_2 + \alpha_R/2}\right) + \log\left(\frac{c_1 + \alpha_R/2}{c_3 + \alpha_R/2}\right) \tag{3.24}$$

where the constants $c_i$ are given in (3.15). This period matches that observed in simulations. This travelling wave is a neutrally stable solution and in simulations, noise eventually perturbs the system into a synchronous solution, which is asymptotically stable.

In order to form a travelling wave, there is a minimum number of oscillators required. This minimum number of oscillators arises from the fact that no two neighboring oscillators can have a time difference larger than the amount of time spent on the middle right branch, $\tau_C$. If there are two neighboring oscillators such that $\Gamma(y_i, y_{i+1}) > \tau_C$, then there will be an instant in time when no oscillators are on the active phase. As a result, one oscillator can travel to the lower left knee and the trajectories seen in Figure 23 cannot be maintained. As a conservative estimate, let us say that the time difference between every neighboring oscillator can be no greater than $\tau_C/2$ if travelling waves are to occur. This implies that the number of oscillators necessary to form a travelling wave, $n_w$, is approximately

$$n_w \sim \frac{2P_M}{\tau_C} \tag{3.25}$$

This approximation appears valid for all tested parameters. Thus, if $\tau_C$ is small in comparison to $P_M$, then the travelling wave will consist of a large number of oscillators arranged in a specific spatial order. If we go to the other extreme and $\tau_C = \tau_B$, which also implies that $B_r = 1$, then only four oscillators (or groups of oscillators) are needed to form a travelling wave. If the initial conditions of the oscillators are randomly chosen, then the probability of forming a travelling wave should be greatest when $\tau_C = \tau_B$. If $\tau_C \ll P_M$, then a travelling wave will require the specific spatial arrangement of a large number of oscillators, which becomes a low probability event using random initial conditions. Our numerical studies support these statements.

It is interesting to consider a limiting case of relaxation oscillators in which the amount of time spent on the right branches goes to zero, $\tau_{URB} \to 0$. As the active phase becomes instantaneous, $\tau_C \to 0$ and approximation (3.25) indicates that the number of oscillators required to form a travelling wave becomes infinite. Therefore travelling waves should not be possible in this limiting case of a relaxation oscillator. Also, as $\tau_{URB} \to 0$, the traversal of the right branch can be thought of as an instant reset to the left branch and the relaxation oscillators become qualitatively similar to integrate-and-fire oscillators, although the pulsatile interaction and the reset rule are different from those specified in Section 2.2. So as an individual relaxation oscillator becomes similar to an integrate-and-fire oscillator, networks of these relaxation oscillators take on properties observed in networks of integrate-and-fire oscillators, namely that travelling waves do not occur (see Chapter 2).

We argue that the travelling waves described here are necessarily a result of the topology of the network. If we use a chain instead of a ring of oscillators, then travelling waves are never observed and logically it does not appear possible for travelling waves to exist.

For a travelling wave to exist, it would need to change directions (reflect) at the ends of the chain, and for a travelling wave to reverse directions it appears to require a complete reversal of the spatial ordering of at least $n_w$ oscillators. We are not aware of a mechanism through which this reordering of $n_w$ oscillators can occur.

In summary, we have graphically described travelling waves. Based on this analysis we have derived the period of a travelling wave and created an approximation for the minimum number of oscillators needed to form a travelling wave. Our understanding of how travelling waves form allows us to choose parameters to either increase or decrease their probability of occurrence when initial conditions are randomly chosen. We have also described why reflections are not possible and therefore that these travelling waves cannot exist in one-dimensional chains of oscillators. We have also formed a link between one limiting case of relaxation oscillators (when $B_r$ becomes infinite) and integrate-and-fire oscillators. In this limiting case, the interactions between relaxation oscillators become instantaneous (as is the interaction between integrate-and-fire oscillators) and the number of oscillators needed to form a travelling wave goes to infinity. Since integrate-and-fire oscillator networks do not exhibit travelling waves, we have further justification for linking relaxation oscillators as $B_r \to \infty$ and integrate-and-fire oscillators.

## 3.5 Synchrony in One-Dimensional Chains

In the previous Section we described two ways in which synchrony does not occur in one-dimensional networks of relaxation oscillators. In Section 3.4.1 we indicated how fractured synchrony could arise if coupling strength is small enough and in Section 3.4.2 we described how travelling waves can arise in a ring of oscillators. We now examine synchrony one-dimensional chains of locally coupled relaxation oscillators.

In order to ensure that synchrony occurs in chains of relaxation oscillators, we use a coupling strength large enough so that fractured synchrony does not occur, i.e. condition (3.21) is satisfied. We do not worry about travelling waves in chains of oscillators because they should not occur without periodic boundary conditions. For a travelling wave to reverse directions would require a complete reversal of the spatial ordering of at least $n_w$ oscillators. Due to this logic, we are convinced that travelling waves do not exist in chains of identical relaxation oscillators. Our data also support this statement.

Section 3.5.1 displays our data indicating that the average time to synchrony $\langle T_S \rangle$ scales as $n^p$, where $n$ is the length of the chain and $p$ is an experimentally obtained quantity which is less than 0.5 for all of our data. We then attempt to explain why $\langle T_S \rangle \sim n^p$ in Section 3.5.2. In Section 3.5.3 we examine the sensitivity of the system to the initial conditions. This section will offer some support for our claims in Section 3.5.2 regarding the scaling relation $\langle T_S \rangle \sim n^p$. We summarize our results in Section 3.5.4. All data in this Section have been obtained in the singular limit ($\varepsilon = 0$) using the singular limit method of Linsay and Wang [Linsay and Wang, 1996].

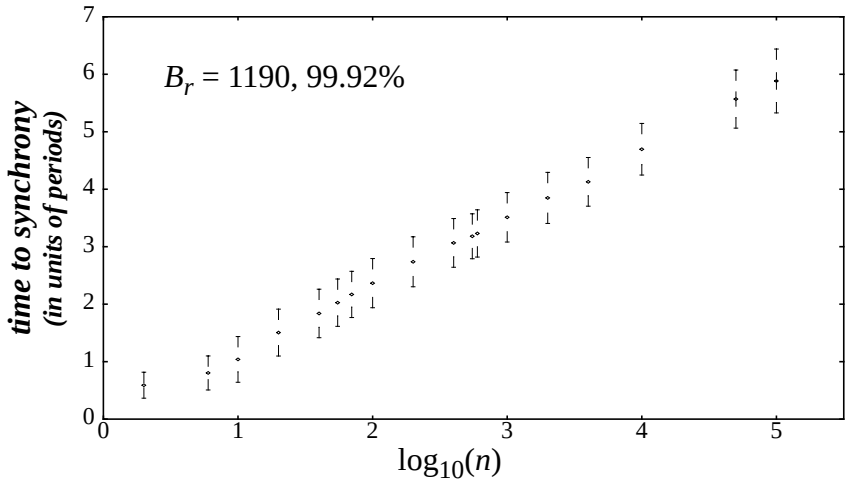


Figure 24. The average time to synchrony for a chain of $n$ relaxation oscillators as a function of $\log_{10}(n)$. The time on oscillator spends on the lower left branch represents 99.92% of the period, or $B_r = 1190$. The error bars are shown and indicate the variance resulting from 500 trials, except for the last two points, which result from 100 and 10 trials respectively. The parameters used are $\lambda = 2079$, $\gamma = 2082$, and $\alpha_R = 3.5$. The initial conditions were randomly distributed on the entire limit cycle.

### 3.5.1 Synchrony in One-Dimensional Networks

We now display our numerical data on synchrony in chains of locally coupled identical relaxation oscillators. Figure 24 displays the average time to synchrony for a chain of $n$ relaxation oscillators as a function of $\log_{10}(n)$, with parameters such that the branch ratio is large, i.e. $B_r = 1190$. For large values of $B_r$ an oscillator spends very little time on the active phase and sends excitation to its neighbors for a very short amount of time. In this respect it is similar to the integrate-and-fire oscillators used in Chapter 2. The resultant qualitative synchronization behavior of these relaxation oscillator networks is the same as that seen for integrate-and-fire oscillator networks, i.e. the average time to synchrony increases with the logarithm of the system size.

As an oscillator spends more and more time on the right branch of the limit cycle, it becomes intuitively less and less similar to an integrate-and-fire oscillator. We examine whether decreasing $B_r$ results in a qualitative change in the average time to synchrony. In Figure 25 we display the average time to synchrony as a function of $\log_{10}(n)$ for several choices of $B_r$ ($B_r = 1190$, $B_r = 19.2$, $B_r = 8.87$, and $B_r = 7.15$). The data indicate that chains with $n < 20$ have the same average synchronization time. For larger chain lengths, networks with different parameters exhibit different times to synchrony. The diamonds ($B_r = 1190$), plus signs ($B_r = 19.2$), and squares ($B_r = 8.87$) all appear to lie on a straight line for values of $n > 100$. The slopes of these lines decrease as the oscillator spends more time on the right branch. We believe that this can be qualitatively explained by noting that the compression ratio, $C_R$, decreases as $B_r \to 1$ (a decrease in $C_R$ increases the rate of syn-

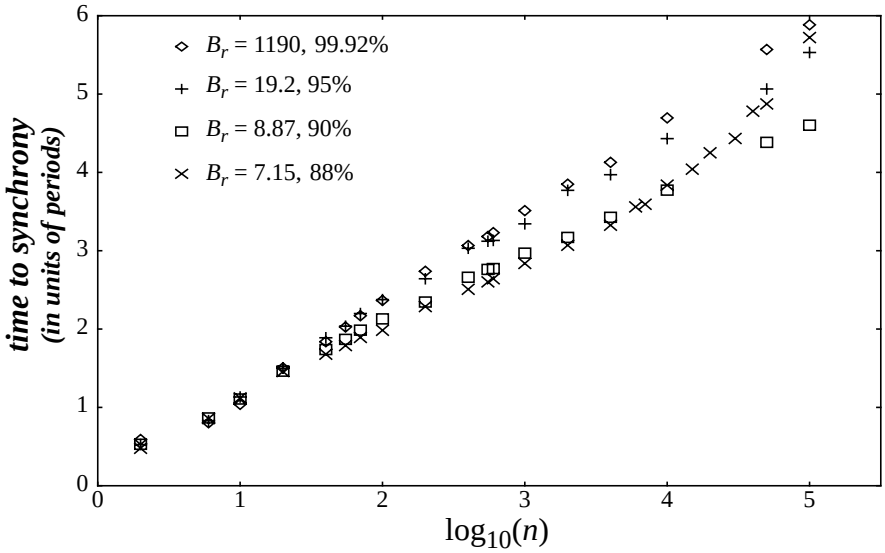


| $B_r$ | $\alpha_R$ | $\lambda$ | $\gamma$ |
|---|---|---|---|
| 1190 | 3.5 | 2079 | 2082 |
| 19.2 | 3.5 | 33 | 36 |
| 8.87 | 3.5 | 16 | 19 |
| 7.15 | 3.5 | 12 | 15 |

Figure 25. The average time to synchrony for chains of $n$ relaxation oscillators as a function of $\log_{10}(n)$. The four different symbols represent four different branch ratios, also indicated are the four different percentages for the amount of time an oscillator spends in the silent phase as compared to the total period. The initial conditions were randomly distributed on the limit cycle.

chronization for a pair of oscillators). The fourth set of data (shown by the "crosses") is for relaxation oscillators with $B_r = 7.15$ and $\langle T_S \rangle$ is no longer linear on this semi-log plot. The compression ratio is smallest for these relaxation oscillators indicating that some other phenomenon occurs which increases $\langle T_S \rangle$ as $B_r$ becomes smaller.

The parameters were chosen specifically to decrease the amount of time an oscillator spends on the right branch without significantly altering other quantities. The other quantities we are interested in maintaining are the size of the jumping region relative to the period, and the coupling strength. By keeping these two quantities similar while widely varying $B_r$, we hoped to observe changes in $\langle T_S \rangle$ that resulted only from varying $B_r$.

We explore synchrony for smaller values of $B_r$. In Figure 26 the trend that started in Figure 25 becomes more pronounced. The average time to synchrony increases significantly as $B_r$ decreases. In Figure 27 we display the same data as shown in Figure 26 except that the data is plotted on a log-log scale. We do not show all of the data from Figure 26 because the average times to synchrony for $n < 100$ do not yield straight lines and we assume that the data for small system sizes does not reflect the asymptotic behavior of the system. For system sizes from $10^2$ - $10^4$, our data indicate that $\langle T_S \rangle \sim n^p$. It is not highly noticeable, but in Figure 27 one can see that the slopes of the lines are slightly different, the points are closer together at the bottom of the graph than at the top of the graph. The slopes of the lines shown in Figure 27 are listed in the table below the figure and vary from a high of 0.46 ($B_r = 1.19$) to a low of 0.14 ($B_r = 7.15$). The data in Figure 27 are somewhat misleading because they give the impression that $p$ is directly related to $B_r$. While it is true in general that $p$ increases as $B_r$ decreases (all of our data support this statement), it is not true that $B_r$ is the only factor controlling the rate of synchrony. Different parameter sets can yield identical values for $B_r$, but the resultant scaling relation between $\langle T_S \rangle$ and $n$ can be quite different. Using the parameters listed at the bottom of the table in Figure 27, results in an average time to synchrony that scales logarithmically with the size of the system, even though $B_r = 3.07$, a value nearly identical to one of the parameter sets shown. We do not have a detailed understanding of how and which parameters are related to $p$, other than the general statement that $p$ increases as $B_r$ decreases. We give some theoretical insight into why this general statement should be correct in the following subsection.

### 3.5.2 Attempt to Explain the Scaling Relation for Relaxation Oscillators

Now that we have this data indicating that $\langle T_S \rangle \sim n^p$ and a rough estimate of how $p$ varies with $B_r$, the task remains of how to explain it. We begin by examining if there are any immediately obvious difference between the behavior of a network with $B_r \gg 1$ and networks with parameters such that $B_r = 1$.

We begin this examination graphically. In Figure 28 we display the temporal evolution of a one-dimensional network of relaxation oscillators with $B_r = 102$ (an oscillator spends 99% of its period on the left branch). Each line represents the time an oscillator jumps up. Because the jump down occurs so quickly after the jump up, the lines representing these events are not visible in Figure 28 due to the thickness of the lines. The oscillators quickly merge and form sizeable blocks within the first cycle. These blocks merge to form larger blocks. However, some oscillators can switch from one block to another. The rectangle

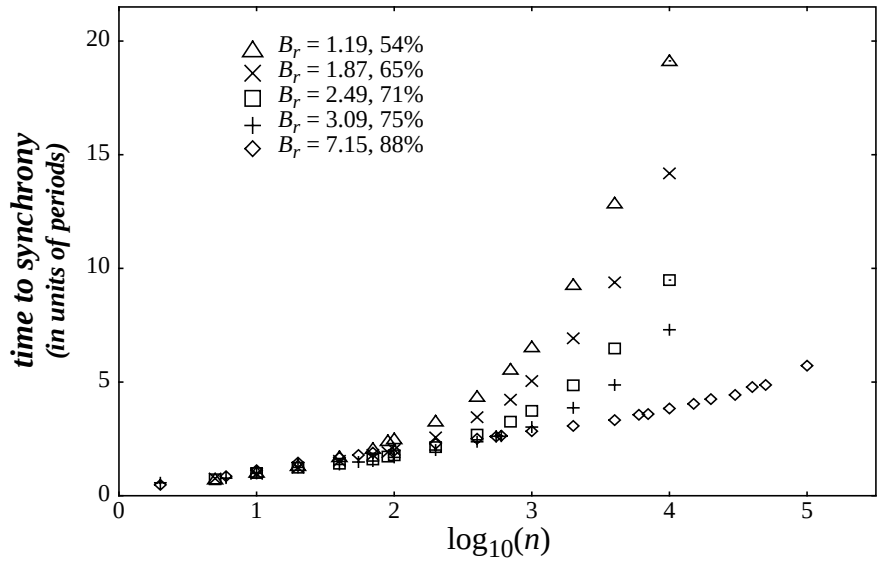


| $B_r$ | $\alpha_R$ | $\lambda$ | $\gamma$ |
|---|---|---|---|
| 7.15 | 3.5 | 12 | 15 |
| 3.09 | 3.5 | 5 | 8 |
| 2.49 | 3.5 | 4 | 7 |
| 1.87 | 3.5 | 3 | 6 |
| 1.19 | 3.5 | 2 | 5 |

Figure 26. The average time to synchronize a chain of $n$ relaxation oscillators as a function of $\log_{10}(n)$ for five different values of $B_r$. The averages are based on several hundred trials. The initial conditions were randomly distributed on the limit cycle.

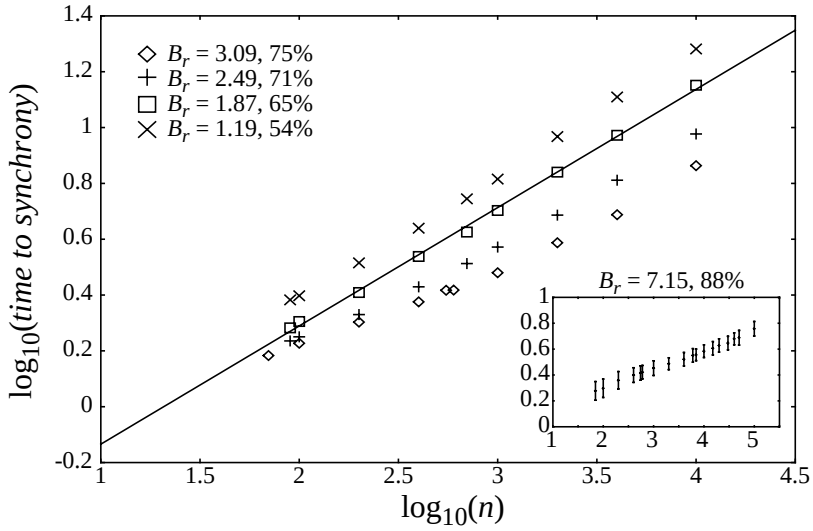


| $B_r$ | $\alpha_R$ | $\lambda$ | $\gamma$ | slope |
|---|---|---|---|---|
| 7.15 | 3.5 | 12 | 15 | 0.14 |
| 3.09 | 3.5 | 5 | 8 | 0.30 |
| 2.49 | 3.5 | 4 | 7 | 0.33 |
| 1.87 | 3.5 | 3 | 6 | 0.45 |
| 1.19 | 3.5 | 2 | 5 | 0.46 |
| 3.07 | 18 | 49 | 80 | N/A |

data not shown

Figure 27. A log-log plot of the time to synchrony as a function of the system size for several different parameters. The inset is the log-log plot for $B_r$ = 7.15 and is shown to indicate the standard deviations associated with each average. Each point corresponds to the average computed from several hundred trials with initial conditions uniformly and randomly distributed throughout the entire limit cycle.

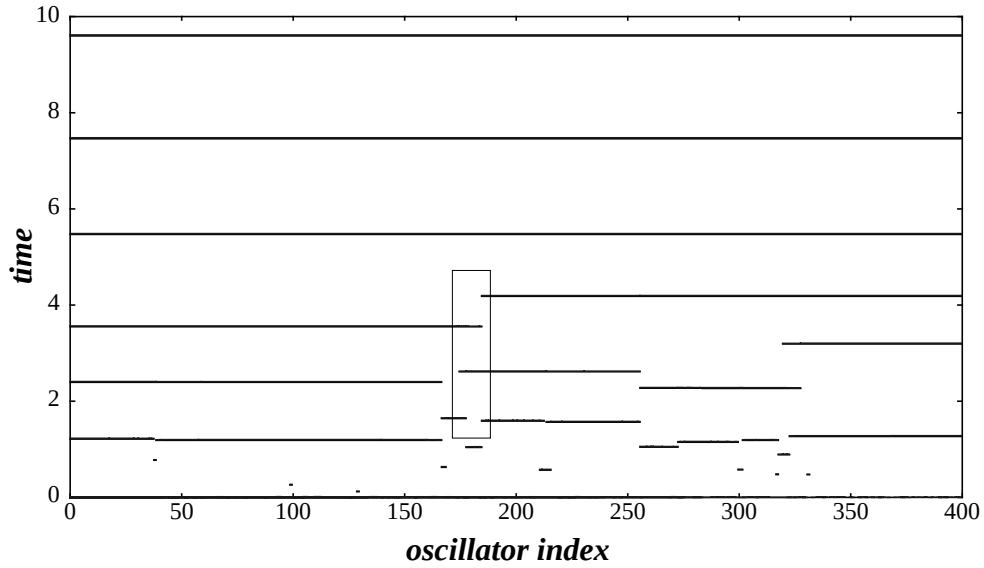


Figure 28. The temporal evolution of a chain of 400 relaxation oscillators with $B_r$ = 102. The thin (thick) lines represent the time each oscillator jumps up (down), but these lines are too close together to distinguish. The rectangle highlights an area where some oscillators fire with different blocks. The parameters used are $\alpha_R$ = 3.5, $\lambda$ = 179, and $\gamma$ = 182. The oscillators were randomly distributed on the limit cycle.

shown in Figure 28 highlights a region in which one can see a number of oscillators which fire with one block, shortly after $t$ = 2; these oscillators then fire with a different block shortly before $t$ = 4. This is different from one-dimensional networks of integrate-and-fire oscillators in which blocks do not break. However, this breaking of blocks is not prominent enough to destroy the overall dynamics that lead to synchronization of the network. Some blocks may become smaller, but the average block size still increases.

We now examine a relaxation oscillator network with $B_r$ = 1. The temporal evolution of a network of 400 relaxation oscillators with $B_r$ = 1 is shown in Figure 29. Both the jumps up (thin lines) and the jumps down (thick lines) are now visible because the oscillators spend a significant percentage of their period (50%) on the active phase. Figure 29 is different from Figure 28 in several ways. One of these differences is that the borders between blocks are no longer sharp. The borders between blocks appear to be of some thickness and they are not corrected, or do not merge with neighboring blocks quickly. Another noticeable feature of Figure 29 is that there are two different frequencies in the system. The synchronous period (about 4 time units) can be seen at the top of the graph when all of the oscillators fire in unison. Another frequency is seen at the ends of the chain (oscillators 300-400 from time 0-10 and elsewhere). From this graph we refer to two types of defects in relaxation oscillator networks. The first defect we call “small defects” and these small defects are rather quickly corrected as blocks of oscillators form. We suggest

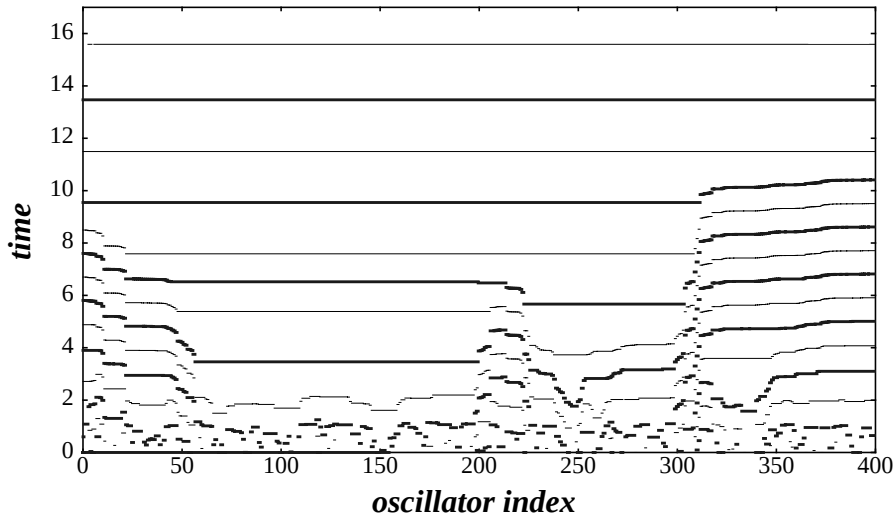


Figure 29. The temporal evolution of a system of 400 relaxation oscillators is displayed. Each thin (thick) dot, or line, represents the time each oscillator (or block of oscillators) jumps up (down). The parameters used are $\alpha_R = 3.5$, $\lambda = 1.75$, and $\gamma = 4.75$, with initial conditions randomly distributed on the entire limit cycle.

that nearly all the small defects are corrected by time $t = 4$. The other defect we refer to as "frequency defects" because they cause the regions of higher frequency. For comparison, Figure 28 contains no frequency defects.

We conjecture that this power law behavior $\langle T_S \rangle \sim n^p$, arises from the frequency defects and that these frequency defects arise from the same types of initial conditions that lead to travelling waves. In support of this conclusion are several facts. The first fact is that the frequency defects have the same frequency as that of the travelling waves. The second fact is that the frequency defects appear to occur most frequently in systems with $B_r = 1$. If $B_r = 1$, then the number of oscillators (or oscillator groups) necessary to create a travelling wave is 4 (using (3.25)). This is the minimum number of oscillators needed to create a travelling wave. Thus, given random initial conditions one would expect frequency defects to occur most often in systems with $B_r = 1$. These facts lead us to believe that frequency defects are the cause of the scaling relation $\langle T_S \rangle \sim n^p$.

How the frequency defects are related to the scaling relation $\langle T_S \rangle \sim n^p$ is as yet unknown. From Figure 29 one can see that frequency defects appear to be corrected when they interact with oscillators that have the synchronous frequency. Where these regions of the synchronous frequency occur and how many of them occur are currently unknown. Since there can be several regions that exhibit the synchronous frequency, the frequency defects can be corrected in many ways. We will later create initial conditions such that there is only one region of oscillators which has the synchronous frequency. This region is located at one end of the chain, thus only one defect at a time can be corrected. Experiments show that for this arrangement, the time needed to synchronize the network is lin-

early dependent on the number of frequency defects. This supports our conjecture that it is the number of regions with synchronous frequencies and their resultant interactions with frequency defects that controls the rate at which a network synchronizes.

We have attempted to come up with other explanations for this power law. So far no evidence supports other possibilities. For example, one can view these defects as boundaries between blocks of oscillators. If the size of the boundaries changed over time, or if the size of the boundaries increased as the size of the system increased, then we could examine this change as a means through which the scaling relation $\langle T_S \rangle \sim n^p$ might arise. However, as one can see in Figure 29, once a defect (or a boundary) exists, there does not seem to be any noticeable change in this boundary until it interacts with a block that has the synchronous frequency. A more careful examination of the boundaries with differently sized networks yields the same conclusion: that the boundary layer does not change in time, or with the size of the system. The fact that these boundaries do not change in time gives support to our conjecture that these frequency defects are related to travelling waves. This is because the time differences between oscillators in a travelling wave are maintained (as discussed in Section 3.4.2).

### 3.5.3 Sensitivity of Relaxation Oscillator Networks to Initial Conditions

In the previous section we indicated that the scaling relation $\langle T_S \rangle \sim n^p$ may arise from frequency defects and their interaction with regions of the synchronous frequency, both of which arise from the initial conditions. This leads us to examine the issue of how sensitive these networks are to initial conditions.

As indicated in Section 3.4.2, one needs a specific spatial relationship between several oscillators to create a travelling wave. Merely shifting the position of a single oscillator in Figure 23 can destroy the travelling wave and the system becomes synchronous. Similarly, shifting the initial position of a single oscillator in Figure 29 can remove one of the frequency defects. If we were to remove the frequency defect near oscillator 225, then one can imagine that oscillators 50-300 become synchronous by time $t = 4$. Because of this change, the entire system could synchronize by time $t = 8$. In tests we have cut the synchronization time of a network in half by altering the initial condition of a single oscillator.

Similarly, one can increase the synchronization time of a network by the creation of frequency defects. Due to the cyclic nature of the travelling waves on the limit cycle, spin wave type initial conditions can create frequency defects. For example, if the wavelength of the spin wave is the size of the system, then there is one frequency defect. If the wavelength is half of the system size then there are two frequency defects, etc. Also, since there is a minimum number, $n_w$, of oscillators needed to create a travelling wave, we infer that there is a similar number of oscillators needed to create a frequency defect. Thus, there should be a maximum number of defects that any one network can contain.When $B_r = 1$ then $n_w \sim 4$ and there can be at most $n/4$ frequency defects in a chain of length $n$. In Figure 30 we plot the time to synchrony for a chain of 500 oscillators (with $B_r = 1$) as a function of the wave number (inverse wavelength). Due to memory constraints, this diagram is a schematic representation of the actual data and the right half of the graph in particular is a caricature of the actual data. We focus on the left half of this graph, which

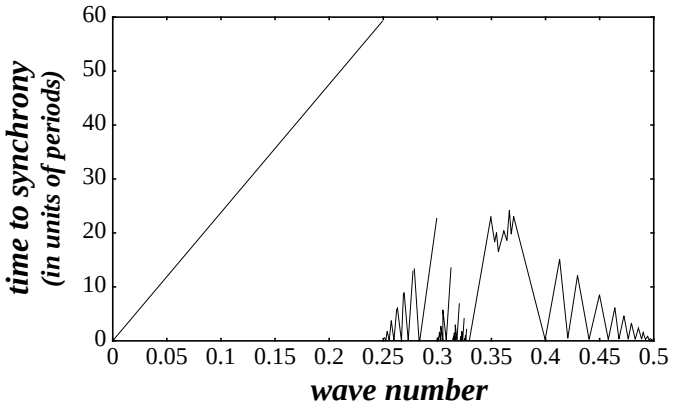


Figure 30. The time to synchrony as a function of the wave number of spin wave type initial conditions in a one-dimensional network of 500 relaxation oscillators. The oscillators were evenly distributed (temporally) on the limit cycle of the travelling wave. The parameters used are $\alpha_R = 5.5$, $\lambda = 2.75$, and $\gamma = 5.75$.

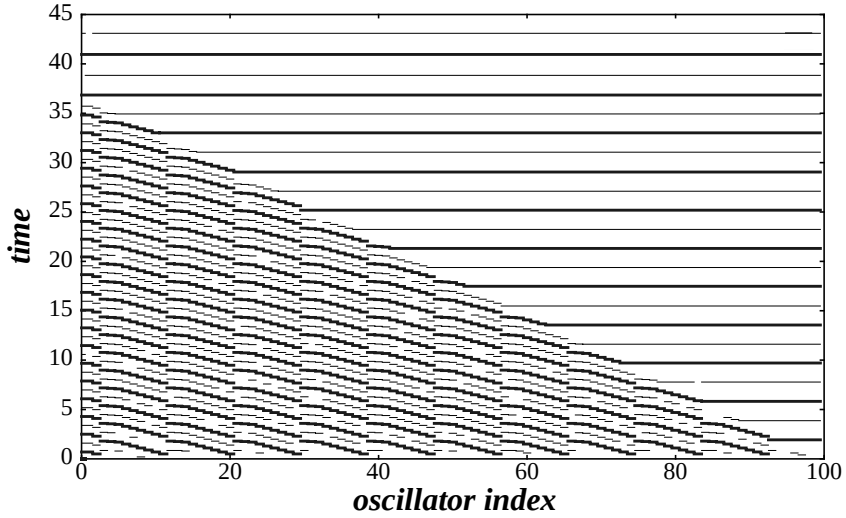


Figure 31. A network of 100 relaxation oscillators with spin wave type initial conditions. Only one region of the synchronous frequency initially forms (at the lower right) and the frequency defects are corrected when they interact with this region. Since there is only one region with the synchronous frequency, only one defect is corrected at a time. The parameters used are $\alpha_R = 3.5$, $\lambda = 1.75$, and $\gamma = 4.75$.

indicates a linear increase in the time to synchrony as the wave number increases. In these trials, one end of the chain begins oscillating at the synchronous frequency of the system, $P_T$. All the other frequency defects are interacting with other frequency defects and are not corrected. This is shown in Figure 31. Since only one frequency defect is corrected at a time, the time to synchrony should increase linearly with the number of defects. The data

in Figure 30 support this statement. The maximum time to synchrony occurs at a wave number of 0.25 (wavelength 4), which is as expected since the maximum number of frequency defects is created at this wave number. For larger value of the wave number, the spin wave type initial conditions do not generate frequency defects in a simple fashion and the graph becomes correspondingly more complex.

### 3.5.4 Summary

In summary we have presented numerical data indicated that $\langle T_S \rangle \sim n^p$ in one-dimensional chains of identical relaxation oscillators without noise. Our data indicate that $p$ increases as $B_r$ decreases. We have examined networks of oscillators in order to find the origin of this scaling relation and in doing so, we have discovered frequency defects. We have shown how these frequency defects can be created and this gives us theoretical insight as to why $p$ should increase as $B_r$ decreases. We have proposed that frequency defects are corrected when they interact with blocks of oscillators that have the synchronous frequency and we have shown some simple cases in which we can control the creation of frequency defects and predict their rates of correction. However, for random initial conditions, the creation of frequency defects and the creation of blocks of oscillators with the synchronous frequency occur unpredictably and we do not know how to accurately estimate even their average quantities. Also, we do not have a complete understanding of how they interact, which we conjecture results in the scaling relation $\langle T_S \rangle \sim n^p$.

## 3.6 Two-dimensional Networks of Relaxation Oscillators

In two-dimensional networks of relaxation oscillators, we again find the three basic behaviors seen in one-dimensional networks; fractured synchrony, travelling waves, and synchrony. With random initial conditions, synchrony is the most frequently observed final state of the system. We also find more complex dynamics than in one-dimensional systems. With periodic boundary conditions (the network is a torus) travelling waves move across the network (up, down, right, and left) and other, more complex spatiotemporal patterns occur. Using normalization (3.17), rotating waves are observed.

In Section 3.6.1 we describe synchronization in two-dimensional networks of relaxation oscillators with parameters such that $B_r \gg 1$. In this limit, the networks exhibit a scaling relation $\langle T_S \rangle \sim \log_{10}(n)$. We describe how the initial conditions can be restricted so that spatiotemporal patterns are never observed. We then graphically describe several types of spatiotemporal patterns in two-dimensional systems in Section 3.6.2.

### 3.6.1 Synchrony in Two-Dimensional Relaxation Oscillators

We now display some of our numerical data on the synchronization time in two-dimensional networks of relaxation oscillators. We first display our data for networks of oscillators in which $B_r = 47.7$ in Figure 32A. For the parameters used, we did not observe rotating waves and synchrony was the final state of the system for all trials. The time to

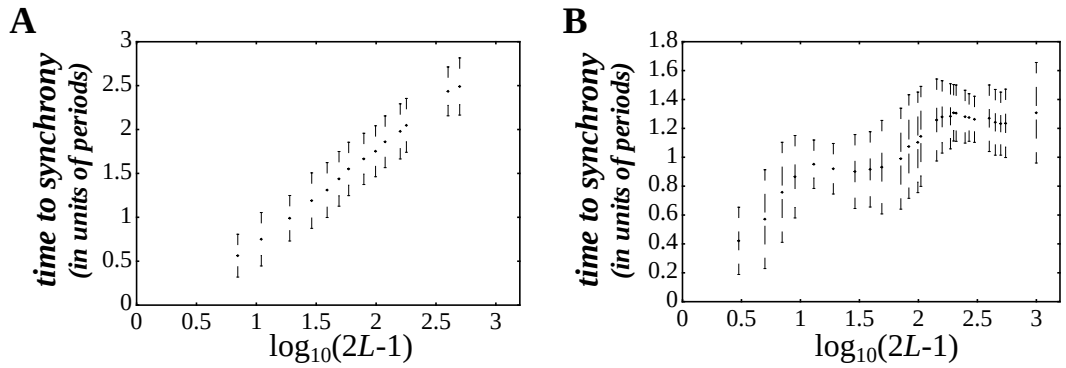


Figure 32. The average time to synchrony in an $L \times L$ network of relaxation oscillators as a function of $\log_{10}(2L\text{-}1)$. (A) A network with parameters such that $B_r = 47.7$ ($\alpha_R = 8$, $\lambda = 112$, and $\gamma = 115$) and the initial conditions were chosen randomly and uniformly from the entire limit cycle. (B) A network with parameters such that $B_r = 3.03$ ($\alpha_R = 8$, $\lambda = 8$, and $\gamma = 11$). The averages are based on several hundred trials and the initial conditions were chosen randomly and uniformly on the lower left branch of the limit cycle.

synchrony yields a straight line on the semi-log plot, indicating that $\langle T_S \rangle \sim \log_{10}(n)$. Rotating waves are possible however, but we believe that they are an extremely low probability event given random initial conditions, using the same arguments presented in Section 3.4.2, namely that a large number of oscillators must have the correct spatial ordering on the limit cycle to form a rotating wave when $B_r \gg 1$.

In Figure 32B we plot a similar graph with parameters chosen such that $B_r = 3.03$. Also, the initial conditions were restricted to lie only on the left branch. With these restrictions on the initial conditions, we have always observed synchrony as the final state of the system. However, even though synchrony is always achieved, there is no longer any apparent scaling behavior. The curve is non-monotonic and non-intuitive. We have no theoretical understanding of how this curve arises. Our data suggest that with initial conditions on the lower left branch, synchronization is bounded above by a quantity proportional to $\log_{10}(2L\text{-}1)$ in an $L \times L$ network. If one allows some oscillators to lie on the right branch, then it is possible for spatiotemporal patterns to form.

### 3.6.2 Spatiotemporal Pattern Formation

Synchrony is not always attained in two-dimensional networks. As in the one-dimensional case, spatiotemporal patterns require a specific set of initial conditions before travelling waves or other periodic behavior form. In one-dimensional systems, at least one oscillator must be on the active phase of the limit cycle at any one time. Also, a travelling wave can consist of blocks of oscillators, or single oscillators. In two-dimensional systems similar logic applies. We display a pattern that appeared in a $4 \times 4$ network of oscillators with periodic boundary conditions in Figure 33. In larger networks, $10 \times 10$ for example, we saw many different types of patterns. Categorizing these patterns remains a topic of

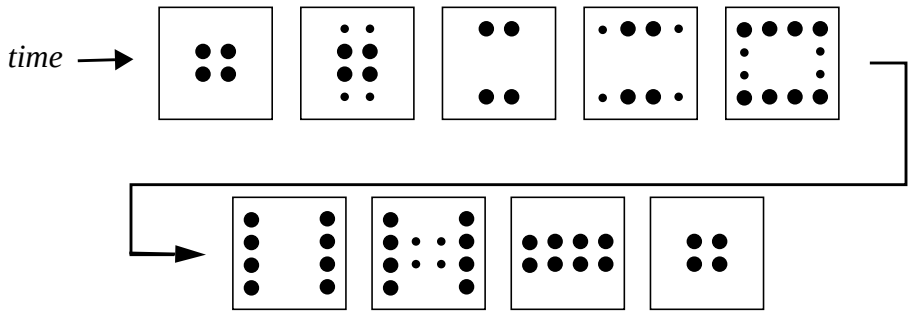


Figure 33. One type of spatiotemporal pattern observed in a network of relaxation oscillators with periodic boundary conditions. The smaller circles represent those oscillators which have recently jumped up to the right branch.The larger circles represent oscillators which are on the right branch of the limit cycle. The parameters used to create this diagram are $\alpha_R = 3.5$, $\lambda = 1.75$, and $\gamma = 4.75$.

interest. The period of these patterns is different from the synchronous frequency of the individual oscillators, and it is also different from the frequency travelling waves seen in one-dimensional systems. In a two-dimensional network with periodic boundary conditions, there are five x-nullclines that an oscillator can lie on dependent on how many oscillators it receives excitation from. The patterns were characterized by one common feature: each group of oscillators was configured such that each oscillator in the group had three nearest neighbors. From this, we surmise that these oscillators travel on the next to the lowest left branch, and the next to the highest right branch, giving a period of

$$P_3 = \tau_{L1} + \tau_{R3} = \log\left(\frac{c_4 + 3\alpha_R/4}{c_2 + \alpha_R/4}\right) + \log\left(\frac{c_1 + \alpha_R/4}{c_3 + 3\alpha_R/4}\right) \tag{3.26}$$

This period matches that observed numerically. We do not know if this is the only period possible in two-dimensional spatiotemporal patterns.

In two-dimensional networks with a grid topology, normalized using (3.17), slightly different types of travelling waves occur. In these systems, we do not see the variety of patterns seen in networks with periodic boundary conditions. We observe only rotating waves. These rotating waves do not have the same period as those in networks with periodic boundary conditions. This is because there are now seven x-nullclines in the system because the weights have more than just a single given value. This period can be described analytically, but we do not get into this detail here. As before, we display a $4 \times 4$ network of oscillators with a highly symmetric rotating wave. In larger systems, rotating waves have the same general pattern, but they may consist of more than four blocks and the center of rotation does not need to be in the center of the network. The waves rotate either clockwise or counter-clockwise. These spatiotemporal patterns are neutrally stable and noise will perturb the system into the synchronous state, which is asymptotically stable.

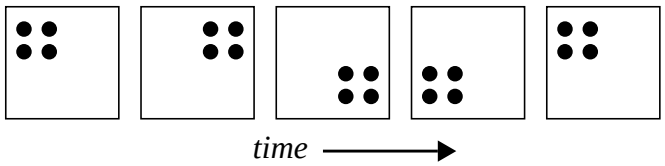


Figure 34. One type of spatiotemporal pattern observed in a network of relaxation oscillators with a grid topology and with connection weights normalized using (3.17). The filled circles represent oscillators which are on the right branch of the limit cycle. The parameters used are the same as in Figure 33.

These patterns do not occur with a high probability when the initial conditions are randomly chosen. When $B_r = 1$ spatiotemporal patterns appear approximately 1/100 trials with random initial conditions. If $B_r = 3$, then a desynchronous solution might result once in $10^4$ trials. If we limit the initial conditions so that the oscillators are only on the lower left branch of the limit cycle, then we observe only synchronous solutions.

We mention these patterns because they might be useful for information processing. Each of the many patterns could represent a stored memory for example. Also, with a more general type of relaxation oscillator in which the speeds along the different branches are different, these spatiotemporal patterns might be stable, as is the desynchronous solutions of a pair of relaxation oscillators [Kopell and Somers, 1995], also see [Terman and Lee, 1997].

## 3.7 Comparison with Integrate-and-Fire Oscillators

Relaxation oscillators are typically thought to have much in common with integrate-and-fire oscillators. Both oscillators used to model neuronal behavior and both are typically examined with a discontinuous interaction. When one relaxation oscillator fires, it can induce its neighbor to fire as well, a dynamic which is similar to that of integrate-and-fire neurons. However, in relaxation oscillators, the interaction is of finite duration, unlike the instantaneous interaction between integrate-and-fire oscillators. Further, in relaxation oscillators the oscillator receiving excitation does not necessarily change its position in phase space, unlike integrate-and-fire oscillators with pulsatile coupling - the oscillator receiving the pulse instantly changes its position in phase space.

Our data indicate that of the differences mentioned, the duration of the interaction is of crucial importance. If the amount of time an oscillator spends on the right branch becomes infinitesimal, or $B_r \to \infty$, then the interaction becomes pulsatile. When an oscillator jumps to the active phase, it makes an instantaneous traversal of the right branch and returns to the top of the left branch. This is similar to the reset mechanism of integrate-and-fire oscillators. However, the interaction is still quite different from that of the integrate-and-fire oscillators. In integrate-and-fire oscillators, the pulse causes an immediate and finite change in the phase of the oscillator receiving the pulse. For relaxation oscillators with $B_r \to \infty$, the interaction either causes an oscillator to jump, or it does not alter its position.

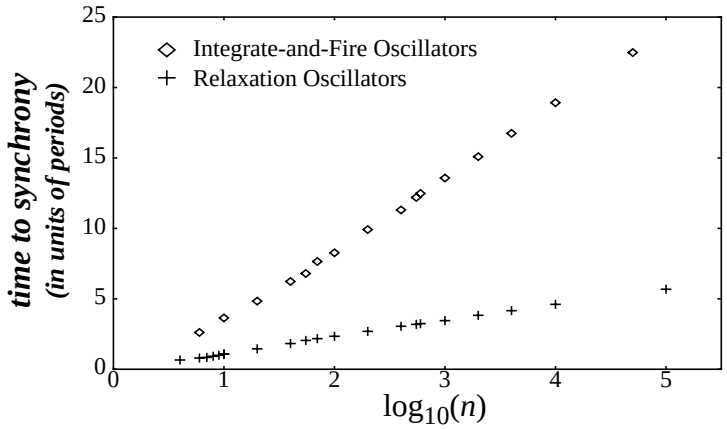


Figure 35. A plot of the average time to synchrony in a chain of $n$ oscillators as a function of $\log_{10}(n)$ for relaxation oscillators with an instantaneous active phase and integrate-and-fire oscillators. Both oscillators have jumping regions which are 70% of the limit cycle and both the data shown is the average of several hundred trials using random initial conditions. The parameters used are $I_0 = 1.11$ and $\alpha_I = 0.2$ for the integrate-and-fire oscillators and $\alpha_R = 3.5$, $\lambda = 4$, and $\gamma = 7$ for the relaxation oscillator.

In Figure 35 we display the average time to synchrony for these two oscillator networks as a function of $\log_{10}(n)$, where $n$ is the length of the chain. The data indicate that both types of oscillator networks synchronize at times proportional to $\log_{10}(n)$. In our comparison of integrate-and-fire oscillator networks and relaxation oscillator networks, we have tried to compare oscillators that exhibit the greatest similarity. We have created an algorithm in which the amount of time spent travelling the right branches is actually zero and we chose parameters so that the size of the jumping region is approximately 70% of the limit cycle for both oscillators. Also, in tests with periodic boundary conditions, travelling waves were not seen in relaxation oscillator networks. This is similar to networks of integrate-and-fire oscillators, in which travelling waves were never seen.

Our data indicate that both types of oscillator networks synchronize at times proportional to $\log_{10}(n)$. However, relaxation oscillator networks achieve synchrony faster than integrate-and-fire oscillator networks. We suggest that this difference may be qualitatively explained by referring to the return maps for two relaxation oscillators (Figure 20A) and the return map for integrate-and-fire oscillators (Figure 5A). The return map for the relaxation oscillators in Figure 20A is not significantly different from the return map for a pair of relaxation oscillators with $B_r \to \infty$. The return map for relaxation oscillators indicates a larger compression per period (in general) and the number of cycles needed before both oscillators can jump together is only one (Figure 20B), while the number of cycles needed for two integrate-and-fire oscillators to fire synchronously can be greater than one (Figure 5B). Based on these return maps alone, one might expect that the time needed to synchronize a chain of relaxation oscillator would be less than the time needed to synchronize a chain of integrate-and-fire oscillators.

## 3.8 Relaxation Oscillators with $\varepsilon > 0$

In the previous sections of this Chapter, the relaxation oscillators were in the singular limit and no time was needed to jump (or hop) from branch to branch. We now investigate relaxation oscillators with $\varepsilon > 0$. There is now a finite amount of time needed for an oscillator to jump from branch to branch. This change immediately causes a fundamental increase in the average time needed to synchronize a network of oscillators. The time needed for one oscillator to induce another oscillator to jump up is finite and information can only propagate from one end of the chain to the other at times proportional to *n*. This was suggested by Somers and Kopell [Somers and Kopell, 1993]. They emphasized the role of relaxation oscillators in obtaining fast synchrony when compared to sinusoidal oscillators. They suggested that when relaxation oscillators are in "the sinusoidal regime, that general invariant manifold theory suggests that phase-pulling mechanisms dominate the behavior." They further noted that in networks of phase oscillators coupled through their phase differences, "the approach to synchrony occurs on the time-scale $O(n^2)$, which is much slower than the time scale suggested above for the relaxation case." Somers and Kopell are clear in their emphasis that sinusoidal oscillators do not synchronize as quickly as relaxation oscillators. However, they are not clear on whether the scaling relation between the time to synchrony and the network size is dependent on the form of the interaction, or the type of oscillator used. In this Section we provide numerical evidence indicating that the type of interaction used can change the scaling relation between the time to synchrony and the size of the system.

We present data indicating that relaxation oscillators with a smoothly varying interaction (3.16.c) with $\kappa = 1$ results in an average time to synchrony proportional to $n^2$. When the coupling is highly nonlinear ($\kappa = 5000$) we observe an average time to synchrony proportional to *n* regardless of whether or not the oscillations are sinusoidal or relaxation like. For $\varepsilon > 0$, it is not possible to use the singular limit method [Linsay and Wang, 1996] and we must use more traditional numerical methods to evolve a network of oscillators. This limits the size of the networks we can examine as well as the number of trials with different initial conditions.

In the singular limit, we defined a network as synchronous when the oscillators all jumped at the same time. For $\varepsilon > 0$, we now need to use a more conventional definition of synchrony. We define a network as synchronous when the average Euclidean distance squared between the oscillators is less than 0.01,

$$0.01 > \frac{2}{n(n-1)} \sum_{i,j<i}^{n} (x_i - x_j)^2 + (y_i - y_j)^2 \tag{3.27}$$

The limit cycle of the oscillator varies in both the x- and y-directions by roughly $O(1)$, thus the threshold chosen in (3.27) indicates that the oscillators are relatively close to each other. We tested several other measures of synchrony and we did not notice any discernible difference in our results.

We used an adaptive fifth order Runge-Kutta method from [Press et al., 1992]. This method was tested against the fourth order Runge-Kutta method with fixed step-size and we found that it was best to modify the adaptive method by placing an upper bound on the step-size. If there is not an upper bound on the step-size, the adaptive method would sometimes take large step-sizes when on the smoothly varying portions of the limit cycle and these large step-sizes could result in unacceptable errors when the oscillators begin to move through the quickly varying portions of the limit cycle. We also compared the results of these numerical methods to results obtained with the Bulrisch-Stoer method of integration, which uses a fundamentally different technique for integration than the Runge-Kutta method. All three methods yield similar numerical results, thus we are confident that our data do not contain significant errors from our numerical procedures.

We present our data in the form of histograms of the time to synchrony for one-dimensional networks. These histograms are based on several thousand trials with the initial conditions randomly distributed on the lower left branch of cubic. .All trials resulted in synchrony. We use parameters so that the speed of motion along the limit cycle is as uniform as possible when ε is $O(1)$. The parameter κ controls the steepness of the slope of the sigmoidal interaction. The parameter ε is used to vary the oscillator from sinusoidal to

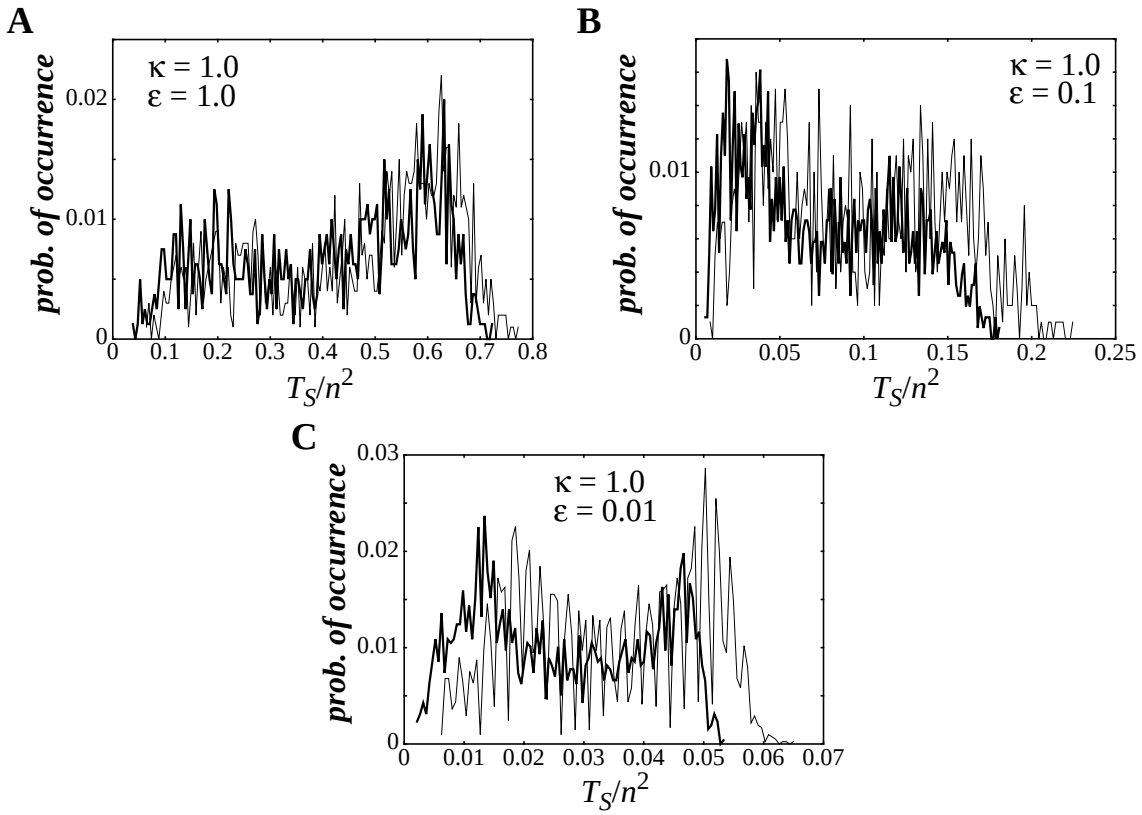


Figure 36. The histograms of the time to synchrony for chains of length $n$ = 25 (thin) and $n$ = 50 (thick). The histograms are scaled by $n^2$. All histograms are based on more than 1000 trials. (A) The scaled histograms for ε = 1.0, (B) ε = 0.1, and (C) ε = 0.01. The other parameters used are $\alpha_R$ = 6, λ = 3, γ = 42, θ = -0.5, and β = 1000.

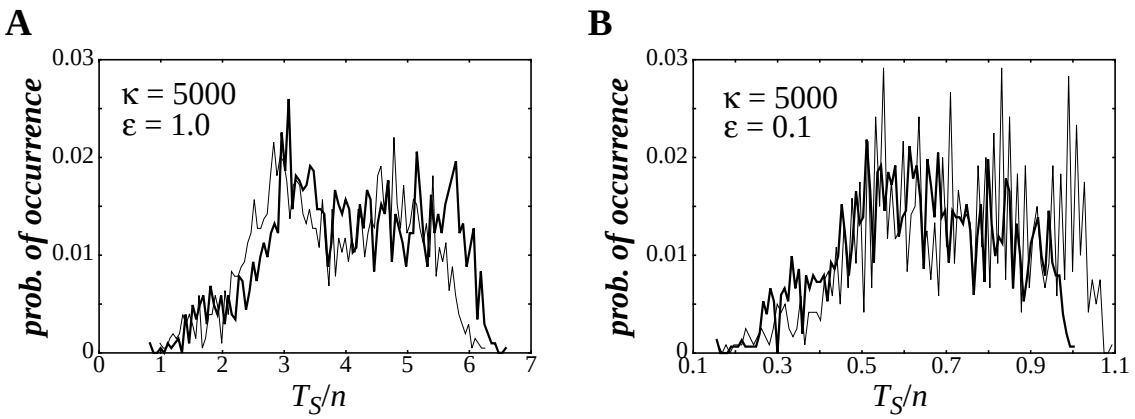


Figure 37. Histograms of the time to synchrony using a highly nonlinear interaction (κ = 5000). The histograms are scaled by the size of the network. Two histograms are shown in each graph and the thin lines represent $n$ = 25 and the thick lines are for $n$ = 50. (A) The histograms for ε = 1.0 and (B) for ε = 0.1. The other parameters are as listed in Figure 36.

relaxation type. We vary ε, κ, and $n$, in order to determine whether it is the interaction, or the type of oscillator that controls the scaling relationship between $\langle T_S \rangle$ and $n$. Figure 36A displays scaled histograms of the time to synchrony for a network of oscillators with ε = 1 and κ = 1, for networks of sizes $n$ = 25 and $n$ = 50.The histograms have been scaled by $n^2$ and it is evident that this scaling is appropriate. Although the histograms are extremely noisy and the variance of the average time to synchrony is quite large, the scaled histograms have a qualitative match in their shape and their extent. Figure 36B displays similar histograms except that ε = 0.1 and the oscillators are more relaxation like. This data also indicate that scaling by $n^2$ is appropriate for this interaction. We also display histograms for ε = 0.01 in Figure 36C. Here there seems to be a discrepancy in that the scaled histogram for $n$ = 50 does not line up precisely with the histogram for $n$ = 25. Scaling by $n^2$ overestimates the time to synchrony. This is as expected because for small ε, the jumps between branches occur quickly and as such the interaction also changes quickly and it behaves like a Heaviside function. We do not yet have enough data to estimate a value of ε that would yield synchronization times proportional $n$ for an interaction with κ = 1.

We now display similar histograms with an interaction term that is virtually discontinuous, i.e. κ = 5000. The histograms are scaled by $n$ in Figure 37. The scaled histograms give good qualitative evidence that $\langle T_S \rangle$ scales linearly with the size of the network, even if the oscillator is sinusoidal. See Appendix A to view the limit cycle and waveform of the oscillator with ε = 1.

Our data confirm the results of Somers and Kopell [Somers and Kopell, 1993] in that relaxation oscillators do exhibit faster synchronization than sinusoidal oscillators. For all values of κ tested, the average time to synchrony decreases as ε decreases, or as the oscillators become more relaxation like (data shown in Figure 38). The data also indicate that

A

| $\kappa = 1$ | $n = 10$ | $n = 25$ | $n = 50$ |
|---|---|---|---|
| $\varepsilon = 1.0$ | 61.0 | 292 | 1050 |
| $\varepsilon = 0.33$ | 31.8 | 149 | 503 |
| $\varepsilon = 0.1$ | 14.7 | 61.5 | 192 |

B

| $\kappa = 5000$ | $n = 10$ | $n = 25$ | $n = 50$ |
|---|---|---|---|
| $\varepsilon = 1.0$ | 35.2 | 96.8 | 179 |
| $\varepsilon = 0.33$ | 15.6 | 37.1 | 70 |
| $\varepsilon = 0.1$ | 7.76 | 18.0 | 32.5 |

Figure 38. We display the average time to synchrony (in units of periods) for different values of $n$, $\varepsilon$, and $\kappa$. (A) is our data for $\kappa = 1.0$ and (B) is our data for $\kappa = 5000$. The data indicate an increase in the time to synchrony as $n^2$ for $\kappa = 1.0$ and as $n$ for $\kappa = 5000$. The data also suggest that the time to synchrony is proportional to $\varepsilon^{2/3}$ for both cases.

the time to synchrony is proportional to $\varepsilon^{2/3}$. This is in agreement with perturbation theory for relaxation oscillators, in which an expansion in $\varepsilon$ gives a first term of order $\varepsilon^{2/3}$ [Bender and Orszag, 1978].

Based on this data we conjecture that a discontinuous interaction has better properties of synchronization than a smooth interaction for many classes of oscillators. This is a bold generalization based on a specific model of oscillation with a specific type of interaction. Our data may include large errors due to boundary effects, or the effects of correlations that are larger than the size of the system used. In spite of these possibilities, we have good reasons to believe in our data. One reason is that the histograms for different $n$ have very similar shapes, indicating that these shapes result from the system parameters and not the size of the network. Also, our data indicate an expected proportionality to $\varepsilon^{2/3}$, and this proportionality might not have been evident if boundary effects were significant.

This conjecture is in agreement with the work of Daido [Daido, 1993b] which indicates that a step-like interaction can perfectly synchronize a portion of the oscillators in a globally coupled network of oscillators with a normal distribution of intrinsic frequencies (whereas a smooth coupling cannot). In Chapter 2 we presented numerical evidence that a network of pulse coupled integrate-and-fire oscillators synchronizes at times proportional to $\log_{10}(n)$ for one- and two-dimensional networks. When integrate-and-fire oscillators are coupled with a smoothly varying function, the scaling relation changes completely. Both Daido's work and the data presented here and in Chapter 2 indicate that a discontinuous interaction induces better properties of synchronization in networks of oscillators than a smooth interaction.

## 3.9 Discussion

We have thoroughly examined locally coupled networks of identical relaxation oscillators with a Heaviside type interaction. The motivation for studying relaxation oscillators with this form of interaction comes directly from neurobiology. Relaxation oscillators

have been derived directly from models of neuronal activity [Fitzhugh, 1961, Nagumo et al., 1962] and the Heaviside coupling mimics chemical excitatory synaptic coupling between neurons. We have examined locally coupled networks because they are more neurobiologically plausible and because theoretically, more interesting computations can be carried out in such networks (see Section 1.5 for a more detailed explanation).

The relaxation oscillators we examine are the Terman-Wang oscillators [Terman and Wang, 1995] that are based on the Morris-Lecar model of neural behavior [Morris and Lecar, 1981]. Networks of these relaxation oscillators contain seven parameters. The most basic of these is $\varepsilon$, the parameter that controls the two different time scales that define relaxation oscillators. If $\varepsilon$ is of $O(1)$, then the oscillator is said to be in the sinusoidal regime because it can have a nearly uniform speed of motion along its limit cycle. As $\varepsilon$ becomes small, the oscillator begins to exhibit two distinct time scales and there is a smooth transition from sinusoidal oscillations to relaxation oscillations. At $\varepsilon = 0$, the relaxation oscillators are said to be in the singular limit, and the two different time scales have an infinite ratio. In the singular limit, one can vary other parameters so that relaxation oscillators begin to take on characteristics of integrate-and-fire oscillators. Common relaxation oscillators, relaxation oscillators in the singular limit, and relaxation oscillators in the pulsatile limit can all approach synchronous solutions and they each have different time scales for this approach.

We have performed analysis in the singular limit indicating that a pair of identical relation oscillators can synchronize given specific initial conditions and if the coupling strength is large enough. We explicitly derived the coupling strength needed for two oscillators to synchronize. We then extended this analysis to indicate what conditions are necessary in order for a one-dimensional chain of oscillators to synchronize. Using this knowledge we then studied the rate of synchronization in one-dimensional networks of relaxation oscillators (also in the singular limit). Our simulations indicate that the average time needed to synchronize increases as $n^p$, where $n$ is the length of the chain and $p$ is an experimentally determined constant that depends on network parameters. Our data indicate that $p$ is related to the branch ratio, $B_r$, of the oscillators, defined as the amount of time an oscillator spends on the lower left branch divided by the amount of time an oscillators spends on the upper right branch. Our data indicates that $p$ increases as $B_r$ decreases (with the minimum value of $B_r$ being 1 and the maximum observed value of $p$ being 0.46). We have made a great deal of progress in understanding the system and we have discussed what we believe to be the underlying causes of this power law, but we have not explicitly derived the scaling relation $\langle T_S \rangle \sim n^p$.

If the amount of time an oscillator spends on the right branch is very small, i.e. $B_r$ is much greater than one, then the oscillator becomes intuitively similar to the integrate-and-fire oscillators studied in Chapter 2. Our numerical studies indicate that as $B_r$ becomes large, the average time to synchrony increase logarithmically with the size of the system, or $p$ in the power law becomes small which makes it appear like a logarithmic increase for the system sizes we are able to examine numerically. This result indicates that by varying the appropriate parameters, networks of relaxation oscillators can exhibit synchronization properties similar to networks of integrate-and-fire oscillators.

Our results reveal the extreme versatility of relaxation oscillators, which, through appropriate parameter choices, can in one extreme appear similar to sinusoidal oscillators, and at another extreme exhibit qualities and behaviors of integrate-and-fire oscillators. Each of these two extremes exhibit different properties from relaxation oscillators in the singular limit, which have their own independent properties of synchronization.

Synchrony in two-dimensional networks of relaxation oscillators is not so easily quantified. If $B_r$ is large, these networks again have synchronization times that scale logarithmically with the system size. If $B_r$ is $O(1)$ then we must constrain the initial conditions appropriately so that rotating waves do not occur. We are unable to characterize the rate of synchronization. From our data, we guess that the rate of synchronization in two-dimensional networks is bounded from above by a logarithmic relation to the size of the network. Parameters can be chosen so that two-dimensional networks synchronize extremely fast, e.g. a $1000 \times 1000$ network can synchronize in less than two periods.

Networks of relaxation oscillators exhibit a wide variety of behaviors - synchrony is not the only final state of the network. In a network with periodic boundaries, we have characterized travelling waves and understood the conditions necessary for their creation. These travelling waves have their own frequency and we can explicitly derive this frequency as a function of system parameters. In two dimensional networks, rotating waves can occur. They can exist in a wide variety of distinct states and this might be useful for information processing. With periodic boundaries, we observe other types of spatiotemporal patterns.

We have also examined networks of identical locally coupled relaxation oscillators using a Heaviside interaction and with finite values of $\varepsilon$. This is a distinctly different regime and networks of oscillators with finite $\varepsilon$ appear to synchronize at times directly proportional to $n$. Somers and Kopell [Somers and Kopell, 1993] suggested this synchronization rate and compared it to sinusoidal oscillators, which typically exhibit synchronization times that are proportional to $n^2$. They noted that relaxation oscillators synchronize more quickly than sinusoidal oscillators but they did not clarify whether or not the scaling relation was dependent on the type of interaction, the nature of the oscillations, or some combination of the two. We have performed numerical experiments indicating that it is the nature of the interaction that determines the scaling relation between the time to synchrony and the size of the network. Based on these results, we conjecture that discontinuous interactions can qualitatively improve the synchronization properties of oscillator networks when compared to smooth interactions. Our conclusion is in agreement with Chapter 2 and with the work of Daido [Daido, 1993b] who indicated that a step-like function could perfectly synchronize a significant fraction of the oscillators in a globally coupled network of phase oscillators with a normal distribution of intrinsic frequencies. Our conjecture may have practical applications besides image processing. Several devices (Josephson junctions and resonance tunneling diodes [Young et al., 1988]) oscillate at megahertz frequencies. However, the output current of both of these devices is very small and there is a need to create devices that can yield a high output current at these frequencies. At the moment, it is unknown how to quickly synchronize the outputs of locally coupled arrays of these devices. Even a partial understanding of how to achieve quick synchrony in the presence of noise and disorder would be valuable. This form of interaction may also be useful in the synchronization of chaotic dynamical systems.